

Linear and Two-Dimensional Infrared Spectroscopic Study of the Amide I and II Modes in Fully Extended Peptide Chains

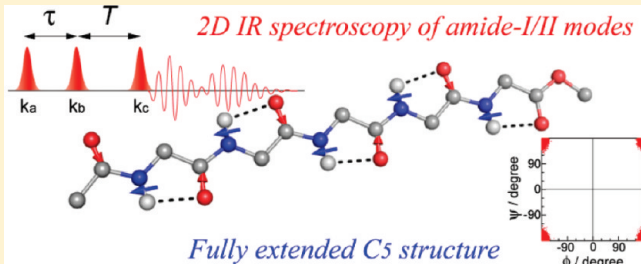
Hiroaki Maekawa,[†] Gema Ballano,[‡] Claudio Toniolo,[‡] and Nien-Hui Ge^{*,†}

[†]Department of Chemistry, University of California at Irvine, Irvine, California, 92697-2025

[‡]Institute of Biomolecular Chemistry, CNR, Padova Unit, Department of Chemistry, University of Padova, 35131 Padova, Italy

Supporting Information

ABSTRACT: We have carried out structural determination of capped C^{α,α}-diethylglycine (Deg) homopeptides with different chain lengths, Ac-(Deg)_n-OtBu ($n = 2-5$), solvated in CDCl₃, and investigated vibrational properties of the amide I and II modes by linear and 2D IR spectroscopy, ONIOM calculations, and molecular dynamics simulations. 2D IR experiments were performed in the amide I region using the rephasing pulse sequence under the double-crossed polarization and the non-rephasing sequence under a new polarization configuration to measure cross-peak patterns in the off-diagonal regions. The 2D IR spectra measured in the amide I and II regions reveal complex couplings between these modes. Model spectral calculations finely reproduced the measured spectral profiles by using vibrational parameters that were very close to the values predicted by the ONIOM method. The agreement led to a conclusion that peptide backbones are fully extended with the dihedral angles (ϕ, ψ) ≈ (±180°, ±180°) and that a sequence of intramolecular C₅ hydrogen bonds forms along the entire chain regardless of the chain length. This conclusion was endorsed by analysis of the molecular dynamics trajectories for $n = 3$ and 5 that showed an exclusive population of the C₅ conformation. The conformationally well-restrained Deg homopeptides serve as an ideal linear exciton chain, which is scarcely obtainable by protein amino acids. We investigated excitonic properties of the linear chain through analytic modeling and compared the measurement and calculation results of the amide I and II modes. The integrated intensity of the amide II band is larger than that of the amide I for the C₅ structure, untypical behavior in contrast with other secondary structures. This comprehensive study characterized the amide I and II spectral signatures of the fully extended conformation, which will facilitate the conformational analysis of artificial oligopeptides that contain such structural motifs.



I. INTRODUCTION

C^{α,α}-dialkylated amino acids^{1,2} are one of the ideal molecular building blocks for designing and synthesizing artificial oligopeptides. They are capable of controlling the molecular structure of the entire peptide chain and specifying the local conformation around certain residues.^{3,4} A well-defined organizational nature is indispensable for the precise replication of designed systems because intramolecular conformation and intermolecular assembly affect their functions and properties to a considerable degree. The allowed conformations and stability of short peptides composed of a family of achiral C^{α,α}-dialkylated glycine⁵ have been extensively studied. For example, C^{α,α}-dimethylglycine or α-aminoisobutyric acid (Aib),^{6–13} which is found in some membrane-active linear peptaibol antibiotics,⁷ is a residue with a high propensity forming 3₁₀- or α-helical structures.^{6–13} A high ratio of Aib residues in the sequence can preferentially induce the 3₁₀-helical structure,⁹ and experiments have shown that capped Aib homopeptides form the 3₁₀-helix over the entire chain in weakly polar solvents^{8,10} as well as in the crystal state.¹¹

When the C^α-carbon has longer alkyl chains attached to it, such as the ethyl groups in C^{α,α}-diethylglycine (Deg)^{14–20} and

the n-propyl groups in C^{α,α}-di-n-propylglycine (Dpg),^{21–24} the bulky side chains lead to the formation of the fully extended C₅ conformation at the residue with the dihedral angles (ϕ, ψ) = (±180°, ±180°). The elongation of the C₅ conformation generates the 2.0₅-helix. An empirical conformational energy calculation predicted that the helical and C₅ structures are two favorable conformations for the Deg and Dpg residues, dependent on the valence angle N–C^α–C'.²⁵ In accord with this prediction, the backbone conformations of Deg- and Dpg-containing peptides have been observed as either fully extended^{14,21} or forming a 3₁₀-helix^{16,17,19,23,24} in the crystalline states. The solution conformations of these Deg and Dpg homopeptides were also studied. Basically, the peptides that are fully extended in the crystalline state keep their backbone conformation in solution.^{15,22} In contrast, some Deg-containing peptides forming the 3₁₀-helix

Special Issue: Shaul Mukamel Festschrift

Received: June 16, 2010

Revised: August 11, 2010

Published: September 16, 2010

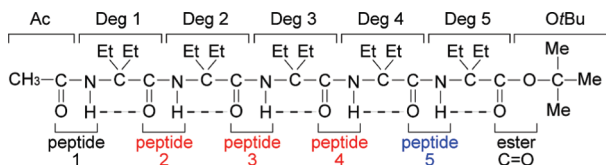


Figure 1. Schematic diagram of Ac-(Deg)₅-OtBu with the fully extended conformation [$(\phi,\psi) = (\pm 180^\circ, \pm 180^\circ)$]. The peptide (amide) –CONH– units in chemically different environments are colored black (between Ac and Deg), red (between Deg and Deg), and blue (between Deg and OEt). Dashed lines represent intramolecular C₅ hydrogen bonds.

in the crystal state, such as Tfa-(Deg)₂-L-Abu-(Deg)₂-OtBu (Tfa, trifluoroacetyl; Abu, α -aminobutyric acid; OtBu, *tert*-butoxy),¹⁷ Tfa-(Deg)₅-OEt (OEt, ethoxy), and Tfa-(Deg)₆-OEt,¹⁹ change their conformation to the C₅ structure in deuterated chloroform.

It should be noted, however, that almost all experimental evidence for determining the solution conformations of C ^{α,α} -dialkylated glycyl homopeptides was based on the NH signal in ¹H NMR measurements and the N–H stretching band of the FT IR spectra in the range of 3200–3500 cm⁻¹.^{8,10,15,18,19,22,24} The lack of C ^{α} H protons due to the two alkyl substituents hindered 2D NOESY and COSY measurements, which are particularly useful in determining the peptide backbone conformation. The ¹H NMR chemical shifts and their dependence on temperature and perturbing agents, such as DMSO (dimethylsulfoxide) and TEMPO (2,2,6,6-tetramethyl-1-piperidylxyl), provided information on solvent accessibility to the amide N–H groups of the peptide units, elucidating their possible participation in intra- and intermolecular hydrogen bonding. The N–H band shape in IR spectra provided qualitative comparisons with those of similar peptides whose structures had already been investigated. This is because the N–H stretching band is altered by the hydrogen bonding effects that make it massively broadened and featureless, which hinders a detailed conformational analysis. Thus, the information acquired by measuring ¹H NMR and FT IR spectra of the N–H groups only provides indirect evidence for inferring the backbone conformation without resorting to physical quantities related to the peptide structure itself. A more direct method needs to be established for the conformational characterization of the C ^{α,α} -dialkylated amino acid residues and oligopeptides in the solution phase.

Our first goal in this paper is to determine the structure of Deg homopeptides, Ac-(Deg)_n-OtBu ($n = 2–5$, Ac, acetyl) in CDCl₃ by linear and 2D IR spectroscopy of the amide I and II modes (Figure 1). The amide I mode, mainly composed of the C=O stretching, has been widely utilized to probe the secondary structure of the peptide backbone because it has a large oscillator strength and exhibits conformation-dependent spectral signatures in linear and 2D IR spectra.^{26–34} In particular, the 2D IR technique allows quantitative evaluation of vibrational coupling strengths, which are directly related to the conformational parameters, such as the distance and angle between different modes. The amide I 2D IR spectral patterns are very sensitive to the vibrational couplings and the underlying peptide conformation. This enabled us to distinguish between two similar structures, such as 3₁₀- and α -helices, whose linear IR spectra resembles one another.^{35,36} The linear amide I peak positions of a series of Tfa-capped Deg homopeptides were previously reported but not discussed in terms of acquiring information on their structure.¹⁵ In this study, we present amide I 2D spectra

taken by the rephasing (R) pulse sequence with the double-crossed polarization configuration^{35,37,38} and the nonrephasing (NR) pulse sequence with a new polarization configuration that reveals the cross-peak pattern in the off-diagonal region instead of the diagonal region.

We expect it to be useful to measure not only the amide I modes but also other modes coupled to them because structural restraints based on various coupling strengths can narrow down the possible structures and the conformational analysis by 2D IR spectroscopy will become more accurate. The amide II mode, consisting mainly of the N–H bending and C–N stretching, serves as one example of this purpose. In fact, some recent 2D IR studies focused on the couplings between the amide I and II modes of *N*-methylacetamide (NMA),^{39–41} small peptides,^{37,42–48} and poly-L-lysine in different secondary structures.⁴⁹ In this study, the amide I/II 2D IR spectra of the Deg homopeptides were also recorded in addition to the amide I cross-peak patterns, from which we determined their conformation. Structural determination was based on whether the simulation of an assumed structure could reproduce all of the measured spectra or not. Such spectral simulation is often required in conformational analysis by 2D IR spectroscopy because observed peaks are typically not assignable to individual amide modes and thus their couplings cannot be evaluated independently. The vibrational exciton model, originally devised to calculate the amide I linear IR spectra of some proteins,⁵⁰ has been refined to compute the amide I 2D IR spectra.^{41,44,51–60} This was applied to both of the amide I and II modes recently.^{47–49,61} Here, we simulated the linear and 2D IR spectra of the Deg homopeptides using this model with initial parameters obtained from ONIOM⁶² calculations.

Having established that the Deg homopeptides adopt the fully extended C₅ conformation by linear and 2D IR spectroscopy, the second goal of this paper is to investigate the spectral properties of the amide I and II modes in this type of structural motif where all peptide units are aligned on the same plane (e.g., Figure 8c). About two decades ago, Cheam and Krimm calculated the amide I and II vibrational properties of *N*-acetylglycine-*N'*-methylamide (Ac-Gly-NHMe) in C₅ and C₇ structures using the 4-21 Gaussian basis set and obtained an unexpected result, namely, that the amide II infrared intensity was larger than the amide I in both the C₅ and C₇ conformations.⁶³ It would be intriguing to experimentally check this unsettled theoretical conclusion because the opposite idea, that the amide I transition strength is larger than that of the amide II, is commonly accepted from an extensive FT IR measurement of biological molecules in the condensed phase.^{26,40,41,57,64–66} However, due to flexibility of the coded amino acids, it was almost impossible to find a fully extended polypeptide chain in the condensed phase. A nonprotected tetrapeptide, FGGF, was one of the two examples taking approximately the fully extended crystal structure with the average dihedral angles of 168.7°.⁶⁷ The other repeating C₅ motif was authenticated for a -(Gly)₄- sequence in histidyl-tRNA synthetase.⁶⁸ The Deg homopeptides in this study served as an ideal system to investigate the excitonic properties of the amide I and II modes in the C₅ conformation.

This paper is organized as follows. Section II briefly outlines the procedures for measuring FT IR and 2D IR spectra, and the experimental results are presented in section III. In the following section IV, protocols of molecular dynamics (MD) simulation, the normal-mode analysis with the ONIOM method, and model calculations of the linear and 2D IR spectra are described. The results are compared with the measurements. Analytic formulas

describing transition frequencies and dipole strengths of a linear exciton chain are summarized, and some fundamental excitonic features as well as pragmatic results for the amide I and II modes are included. In section V, we determine the molecular structure of the Deg homopeptides and analyze their conformational flexibility. Vibrational couplings and frequency distributions are discussed in relationship with available theoretical models. We discuss the spectral features of the amide I and amide II modes observed for the fully extended polypeptide chain and compare them to those of some Aib-rich 3_{10} -helical peptides. Concluding remarks of this study are given in section VI.

II. EXPERIMENTAL SECTIONS

A. Materials. The homopeptides Ac-(Deg)_n-OtBu ($n = 2–5$) were synthesized by reference to previous works^{69,70} and identified with mass spectra and ¹H NMR measurements. Deuterated chloroform (99.96%D, Cambridge Isotope Laboratory) was used without further purification and desiccation. Peptide solutions with $\sim 10–15$ mM concentration were prepared and held in a 180 μm thick sample cell. Previous measurements on the Tfa-capped Deg homopeptides demonstrated that their FT IR spectra remained unchanged in the concentration range of 0.5–50 mM in CDCl₃.¹⁵ We also checked that Ac-(Deg)₅-OtBu exhibits the same FT IR spectra at 1 and 10 mM.

B. Linear and 2D IR Measurements. Linear IR spectra of the peptide solutions and neat CDCl₃ were recorded using a FT IR spectrometer (Nicolet 860, Thermo Scientific) with a 4 cm⁻¹ resolution and averaged over 64 scans under dry air purging. The solvent background spectrum was subtracted from the sample spectra. The peak absorbances of the amide I and II modes were about 0.19 and 0.25, respectively, for example, in the spectrum of Ac-(Deg)₂-OtBu.

Since previous articles already noted details of our 2D IR spectrometer, data acquisition, and processing,^{36,37,47,71} we only briefly describe the 2D IR experimental parameters for the peptides in this study. Three 100 fs IR pulses with wavevectors k_a , k_b , and k_c were focused onto the sample solutions. An induced third-order nonlinear signal was measured using a spectral interferometric method with a combination of a monochromator and a 64 element MCT array detector. Polarization directions of the three IR pulses (a, b, and c for the k_a , k_b , and k_c pulses) and that for the signal (d) are denoted as $\langle a, b, c, d \rangle$. Rephasing (R, a–b–c) and nonrephasing (NR, b–a–c) pulse sequences were generated by adjusting the delay time τ between the first and second pulses and the delay time T between the second and third pulses. In both R and NR measurements, τ was scanned from 0 to ~ 3 ps with a 9 fs time step. The waiting time T was set to 0 for R under the double-crossed $\langle \pi/4, -\pi/4, Y, Z \rangle$ and for NR under the $\langle \pi/4, Y, -\pi/4, Z \rangle$ polarization configuration, and it was set to 300 fs for both R and NR under $\langle Y, Z, Z \rangle$ to minimize the nonresonant solvent response. The local oscillator pulse preceded the signal by 800 fs in order to facilitate the following data processing. The frequency axis ω_τ in the 2D IR spectra was obtained by Fourier transform along τ , and ω_t was experimentally determined at each element of the array detector. The central frequency of the IR pulse was tuned to ~ 1666 cm⁻¹ to measure the amide I cross-peak patterns. In measuring the amide I/II 2D IR spectra, it was set to ~ 1570 cm⁻¹ so that both the amide I and amide II bands were excited with almost the same intensity of the IR pulses. All spectra were collected at ambient temperature ($20 \pm 1^\circ\text{C}$).

III. EXPERIMENTAL RESULTS

A. Chain Length Dependence of FT IR Spectra. Figure 2a shows the measured (solid lines) FT IR spectra of Ac-(Deg)_n-OtBu ($n = 2–5$) dissolved in CDCl₃. All of the spectra were normalized by the peak absorbance of the ester C=O stretching band at ~ 1718 cm⁻¹ after subtracting the solvent background spectrum. Other characteristic IR-active bands shown in the figure are assignable to the amide I ($1620–1700$ cm⁻¹), the amide II ($1460–1540$ cm⁻¹), and the methyl deformations (~ 1460 cm⁻¹) according to the normal-mode analysis with the ONIOM method (see section IV.B).

The Deg homopeptides have two peaks in the amide I frequency region. Their frequency separation ($\Delta\tilde{\nu}_{\text{I,peak}}$) increases from 22.0 ($n = 2$) to 29.3 cm⁻¹ ($n = 5$). It appears that $\Delta\tilde{\nu}_{\text{I,peak}}$ has not reached convergence at the longest chain length available in our measurement (Figure 2b, red circles). The integrated area intensity of the overall amide I bands also increases with the chain length, as expected (Figure 2c, red circles).

The amide II band, consisting of a strong single peak and an elongated shoulder to the higher-frequency side, also gradually changes with the chain length. The peak frequency ($\tilde{\nu}_{\text{II,peak}}$) decreases by more than 10 cm⁻¹ from $n = 2$ (1497 cm⁻¹) to 5 (1486 cm⁻¹), as seen in Figure 2b (blue, circles). The amide II band area, which was evaluated by fitting its line shape together with the methyl deformation bands first and then segregating only the integrated area of the amide II band, exhibits a monotonic increment with n (Figure 2c, blue circles). One of the most interesting features in the FT IR spectra is the relative integrated area ratio between the amide I and II bands ($I_{\text{I}}/I_{\text{II}}$). It is 0.96, almost equal intensity, for the dipeptide and decreases to 0.77 for the pentapeptide, meaning that the amide II band gains more intensity than the amide I as the chain becomes longer (Figure 2c, black).

B. Amide I Cross-Peak Patterns. The left column of Figure 3 shows the absolute magnitude R spectra of the amide I modes measured with $\langle \pi/4, -\pi/4, Y, Z \rangle$. This polarization is capable of suppressing diagonal peaks, and therefore, cross-peaks appear more prominent in the 2D spectrum.⁷² There are two clear peaks for $n = 2$ in the off-diagonal region, one at $(\omega_\tau, \omega_t) \approx (-1673, 1651)$ cm⁻¹ and the other at $(-1654, 1673)$ cm⁻¹. The cross-peak profiles for the longer chains ($n = 3–5$) are similar, and the peak separation between the two peaks is greater than that of $n = 2$. It is difficult to discern cross-peaks between the amide I and the ester C=O modes in those spectra.

The amide I NR cross-peak patterns measured with $\langle \pi/4, Y, -\pi/4, Z \rangle$ are plotted in the left column of Figure 4. Two dominant cross-peaks appear in the off-diagonal regions. This behavior is because cross-peaks in the diagonal region are suppressed in this polarization (see section IV.C), in great contrast with the previous NR cross-peak patterns obtained using the double-crossed $\langle \pi/4, -\pi/4, Y, Z \rangle$ configuration.^{37,38} Comparing Figure 4 to Figure 3, the main differences from the spectra measured with the R sequence are the broadening of the two peaks along the ω_τ axis and the appearing of a trench between the two peaks in longer chains ($n = 4$ and 5). The NR pattern seems to converge from $n = 3$, as is the case for R. Weak off-diagonal peaks at $(\omega_\tau, \omega_t) \approx (1729, 1641)$ and $(1716, 1672)$ cm⁻¹ recorded for $n = 2$ are attributed to coupling to the ester C=O mode, considering their frequency positions. These peaks are not discernible in the corresponding R spectrum in Figure 3.

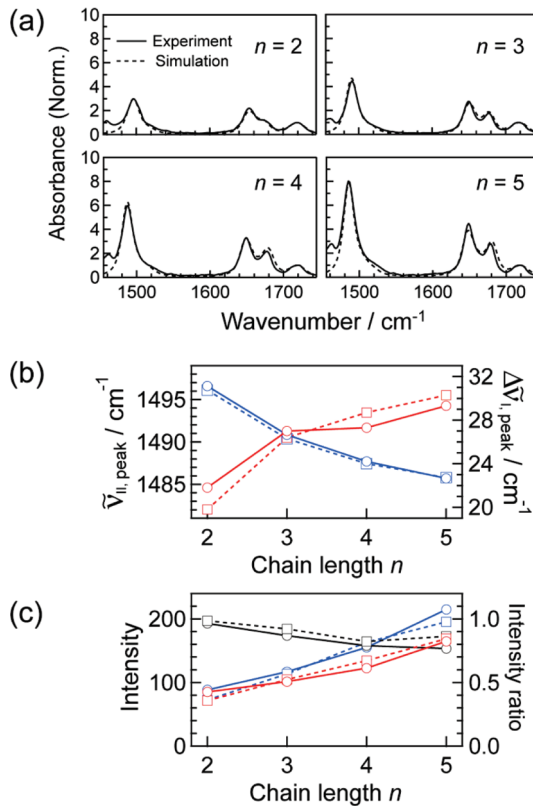


Figure 2. (a) Measured FT IR spectra (solid) of the $\text{Ac}(\text{Deg})_n\text{-OtBu}$ ($n = 2-5$) peptides in CDCl_3 . Each spectrum was normalized by the peak absorbance of the ester $\text{C}=\text{O}$ band at $\sim 1718 \text{ cm}^{-1}$ after subtracting the solvent background spectrum. Simulated linear IR spectra (dashed) are superimposed on the measured spectra after following the same normalization procedure. (b) Frequency separation between the two amide I bands ($\Delta\tilde{\nu}_{\text{I,peak}}$ red) and the peak frequency of the amide II band ($\tilde{\nu}_{\text{II,peak}}$ blue) in the measured (circles) and simulated (squares) linear spectra. (c) Integrated area intensity of the amide I (red) and II (blue) bands and their ratio $I_{\text{I}}/I_{\text{II}}$ (black) in the measured (circles) and simulated (squares) linear spectra. The solid and dashed lines through the markers in panels (b) and (c) are guides for the eyes.

C. Amide I/II 2D IR Spectra. The R spectra of the amide I and II modes collected with $\langle Y, Y, Z, Z \rangle$ are presented in the left column of Figure 5. All of the spectra were normalized by the largest amplitude of the diagonal amide II peak. In contrast to the spectral patterns in Figures 3 and 4, two diagonal peaks are clearly observed in the amide I frequency region, along with the two cross-peaks between them. The amide II diagonal peak is elongated upward along the ω_t axis, to the right along the ω_τ axis, and also along the diagonal. The diagonal elongation is most likely due to the presence of a shoulder at the higher-frequency side observed in the FT IR spectra (Figure 2a). The elongation along the frequency axes can be a result of the tails of the diagonal peak and/or cross-peaks between the main peak and the shoulder. Several weak cross-peaks between the amide I and II modes appear at around $(\omega_v, \omega_t) \approx (-1650, 1490)$ and $(-1480, 1650) \text{ cm}^{-1}$. It should be noted that the diagonal peak at $(-1600, 1599) \text{ cm}^{-1}$ and the anharmonically shifted peak at $(-1600, 1571) \text{ cm}^{-1}$ come from the bending mode of trace H_2O molecules in CDCl_3 solvent. The peak intensity of the bending mode appears strong because it was excited by the most intense part of the IR pulse spectrum centered at $\sim 1570 \text{ cm}^{-1}$.

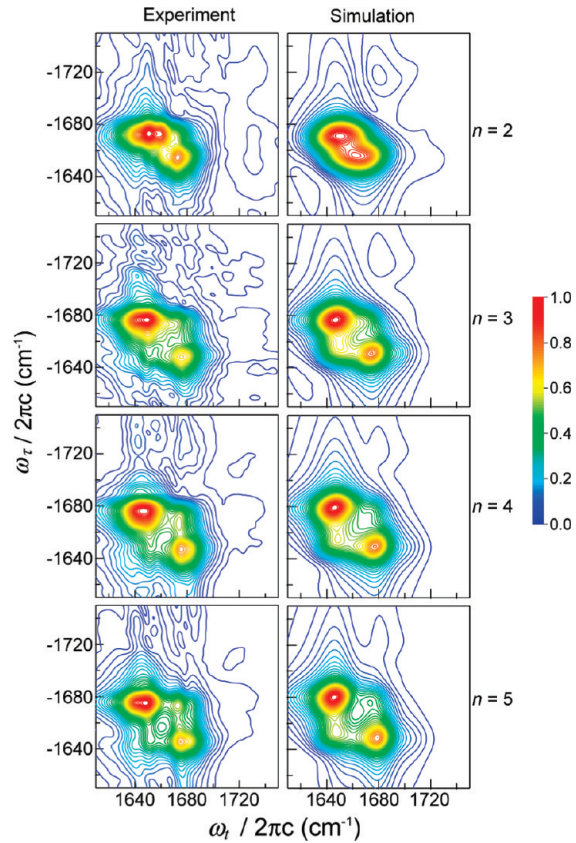


Figure 3. Measured (left column) and simulated (right column) absolute magnitude 2D IR amide I spectra of $\text{Ac}(\text{Deg})_n\text{-OtBu}$ ($n = 2-5$) in CDCl_3 with the R pulse sequence and $\langle \pi/4, -\pi/4, Y, Z \rangle$ polarization configuration. Each spectrum is normalized by the maximum amplitude and plotted with 40 equally spaced contour lines from 0 to 1.

Figure 6 shows the perpendicular amide I/II NR spectra, normalized by the diagonal amide II peak amplitude. Spectral patterns are similar to those observed with the R sequence, except that the diagonal amide I and II bands are not notably extended along the diagonal and the cross-peak intensities between the amide I and II modes are higher in the NR spectra.

IV. COMPUTATIONS

In this section, we summarize calculation protocols and results and the theoretical analysis for structure determination of the Deg homopeptides based on the measured linear and 2D IR spectra.

A. MD Simulations. We utilized a comprehensive MD simulation package, NAMD,⁷³ to compute trajectories of $\text{Ac}(\text{Deg})_3\text{-OtBu}$ and $\text{Ac}(\text{Deg})_5\text{-OtBu}$ in CDCl_3 based on AMBER ff99SB force fields.^{74,75} Torras et al. used the same force fields to run MD simulation of Tfa-capped Deg pentapeptides and studied their backbone conformations.⁷⁶ We employed the electrostatic parameters of the Deg residue reported in that study and those of *tert*-butyl ester in our previous work.⁴⁸

One tri(penta)peptide in a $57 \times 48 \times 46$ ($62 \times 51 \times 48$) Å rectangular box containing 911 (1086) CDCl_3 molecules was equilibrated for 3.5–4.0 ns under constant temperature (293 K) and pressure (1.0 atm), regulated by the Langevin dynamics method with a damping coefficient of 5 ps^{-1} ⁷⁷ and Langevin

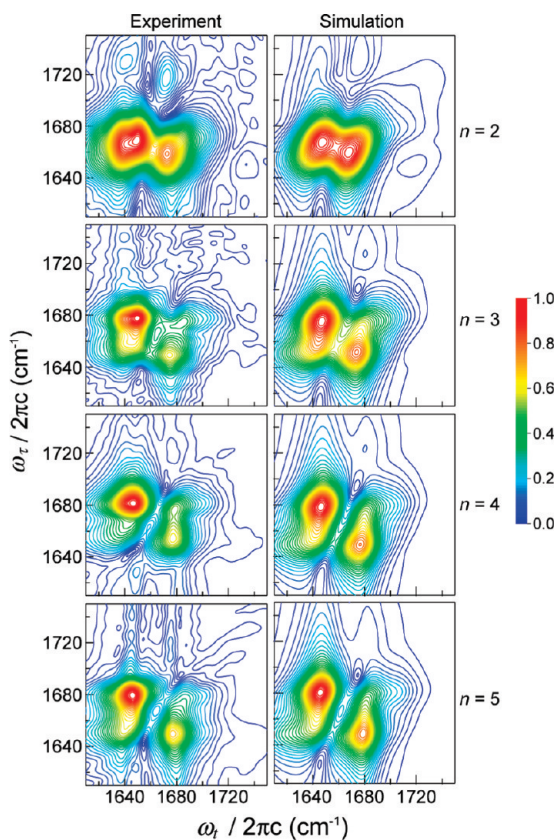


Figure 4. Measured (left column) and simulated (right column) absolute magnitude 2D IR amide I spectra of $\text{Ac}(\text{Deg})_n\text{-OfBu}$ ($n = 2-5$) in CDCl_3 with the NR pulse sequence and $\langle \pi/4, Y, -\pi/4, Z \rangle$ polarization configuration. See the caption of Figure 3 for other details.

piston Nosé–Hoover barostat,^{77,78} respectively. Benedetti, Tonoli, and co-workers determined the crystal structures of $\text{Tfa}(\text{Deg})_n\text{-OfBu}$ ($n = 1-5$) with X-ray diffraction analysis,¹⁴ and the corresponding structures of $n = 3$ and 5 were utilized as the initial structures in our MD simulation. The dihedral angles ϕ and ψ of the crystal structures are presented in Table 1. Electrostatic interaction was calculated by the particle-mesh Ewald sum method.⁷⁹ The nonbonded cutoff distance was set to 14 Å. All bond lengths involving hydrogen atoms were constrained using the SHAKE algorithm.⁸⁰ The trajectory was calculated with a 2 fs time step in production runs, and 150 000 snapshots were sampled at every 0.1 ps along the 15 ns trajectory for the analysis of the molecular conformations.

Table 1 summarizes the average dihedral angles and standard deviations for each peptide unit obtained from the 15 ns MD trajectory analysis for $n = 3$ and 5 (the Ramachandran plots are shown in Figure S1, Supporting Information). The production run in CDCl_3 resulted in an exclusive population of the C_s conformation at around $(\phi, \psi) = (\pm 180^\circ, \pm 180^\circ)$, with standard deviations of $7.0-13.4^\circ$. Torras et al. had obtained similar Ramachandran plots for $\text{Tfa}(\text{Deg})_5\text{-OfBu}$ in their MD simulation study.⁷⁶ Our simulation results show that the tripeptide is only slightly more flexible than the pentapeptide and also that fluctuations of ψ at the C-terminus unit are larger than those of the other angles.

Table 2 lists three structural parameters of the intramolecular hydrogen bonds in the C_s conformation, the two distances $\text{N}\cdots\text{O}$ and $\text{H}\cdots\text{O}$ and the angle $\angle\text{NHO}$ of each residue. In

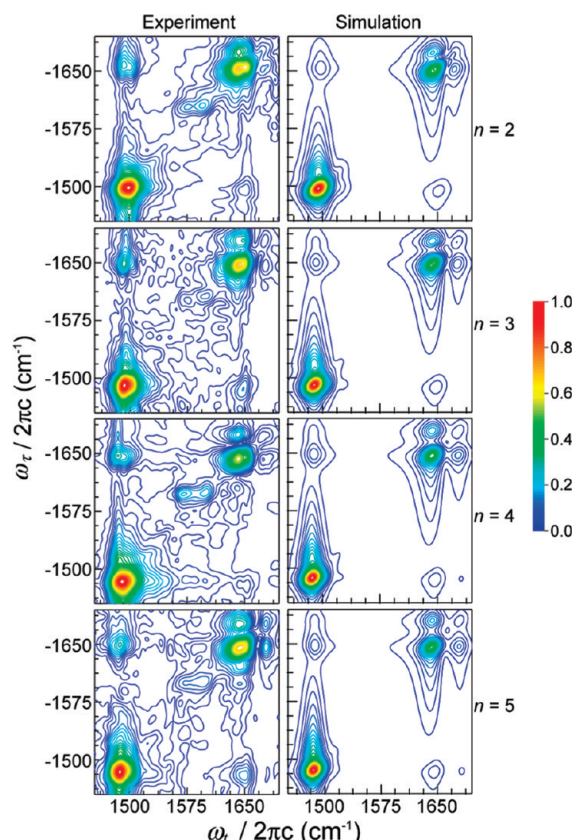


Figure 5. Measured (left column) and simulated (right column) absolute magnitude 2D IR amide I/II spectra of $\text{Ac}(\text{Deg})_n\text{-OfBu}$ ($n = 2-5$) in CDCl_3 with the R pulse sequence and $\langle Y, Y, Z, Z \rangle$ polarization configuration. Each spectrum is normalized by the maximum amplitude of the diagonal amide II band and plotted with 40 equally spaced contour lines from 0 to 1.

the MD trajectories, the average distances become slightly longer than those observed in the crystal state of the Tfa-capped peptides. Although there is no significant chain length dependence in the distances, the simulation results show an interesting trend that the distances, especially of $\text{H}\cdots\text{O}$, alternate in length along the peptide chain. Compared to the crystal structures, the average angle $\angle\text{NHO}$ in the simulation is smaller, but the angle differences between the trajectories and the crystal state are almost within the standard deviations of the simulation.

B. Vibrational Properties from ONIOM Calculations. The amide I/II linear and 2D IR spectra of the Deg homopeptides were calculated based on a vibrational exciton model,⁵¹ as described in the next subsection. Building the exciton Hamiltonian, that is, setting the local-mode energies and vibrational couplings, is the most important step in the model calculation. It has been realized that the local environment around a peptide unit, such as intra- and intermolecular hydrogen bonding and solvent interactions, significantly affects the amide frequencies.^{40,44,65,81} An implicit assumption of constant local-mode frequencies over the entire peptide chain is not adequate. In the Deg homopentapeptide chain, for example, there are three different types of local environments around the peptide (amide)-CONH- units when it takes the fully extended conformation, as shown in Figure 1: the peptide unit between two Deg residues (unit 2–4, red) in which both the $\text{C}=\text{O}$ and $\text{N}-\text{H}$ groups form C_s hydrogen bonds with other Deg residues, the

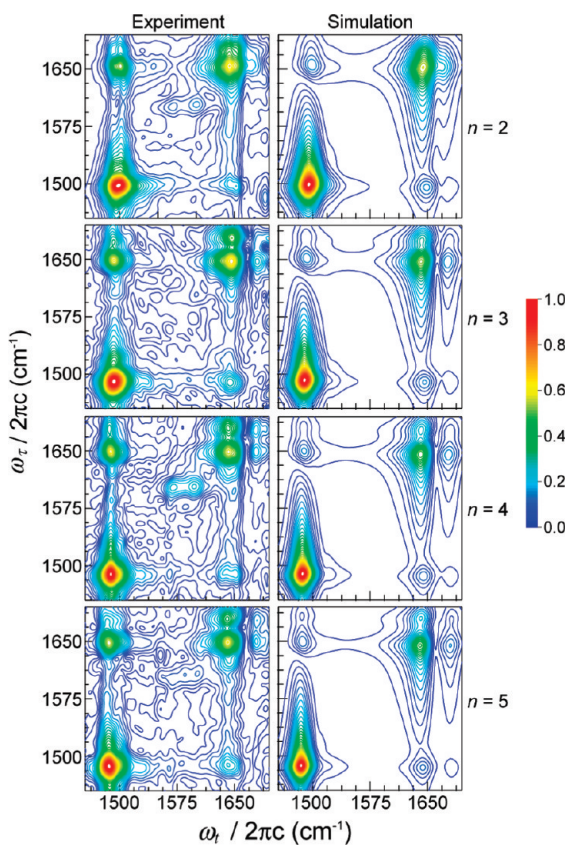


Figure 6. Measured (left column) and simulated (right column) absolute magnitude 2D IR amide I/II spectra of $\text{Ac}(\text{-Deg})_n\text{-OtBu}$ ($n = 2\text{--}5$) in CDCl_3 with the NR pulse sequence and $\langle Y, Y, Z, Z \rangle$ polarization configuration. See the caption of Figure 5 for other details.

unit between the Ac and Deg residue (unit 1, black) whose carbonyl group is free from the intramolecular C_5 hydrogen bond, and the last unit between two Deg residues at the C-terminus (unit 5, blue), whose N–H group is hydrogen bonded with the ester carbonyl group.

We carried out quantum mechanical calculations to find out differences in the local amide I and II mode frequencies of these units. Structural optimization and normal-mode analysis of $\text{Ac}(\text{-Deg})_n\text{-OtBu}$ ($n = 2\text{--}5$) were conducted with the backbone dihedral angles fixed at 180° , using the ONIOM method⁶² implemented in the Gaussian 03 package.⁸² The AM1 semiempirical method was applied to the atoms in the ethyl side chains and the three methyl groups of the capping *tert*-butyl group. The DFT method at the B3LYP/6-31+G(d) level was applied to all other atoms. A peptide unit was isolated by isotope substituting the ^{12}C , ^{16}O , and H atoms of the other peptide units with ^{13}C , ^{18}O , and D to obtain the local-mode frequencies in each unit. Table 3 summarizes the local-mode frequencies scaled by a factor of 0.9774 for the ester $\text{C}=\text{O}$ stretching and the amide I modes and 0.9665 for the amide II modes,⁸³ as well as their transition dipole derivatives.

The resulting frequencies and dipole derivatives of the amide I modes indicate three different types of peptide units, consistent with our expectation. The frequencies and transition dipole derivatives of the first units at the N-terminus are $1684\text{--}1685\text{ cm}^{-1}$ and $2.7\text{--}2.8\text{ D Å}^{-1}\text{ amu}^{-1/2}$ for $n = 2\text{--}5$. This occurred partially because the $\text{C}=\text{O}$ group of these units is free from the C_5 hydrogen bond so that their frequencies are higher than those

of the other units. The units between two Deg residues have frequencies of $1669\text{--}1673\text{ cm}^{-1}$ and dipole derivatives of $2.5\text{--}2.6\text{ D Å}^{-1}\text{ amu}^{-1/2}$ for $n = 3\text{--}5$. Most likely, the C_5 hydrogen bonds at the $\text{C}=\text{O}$ and N–H groups make these frequencies the lowest among the three different groups. The last units at the C-terminus show frequencies in the range of $1675\text{--}1678\text{ cm}^{-1}$ and derivatives in $2.2\text{--}2.4\text{ D Å}^{-1}\text{ amu}^{-1/2}$. The vibrational properties reflect subtle environmental differences around similar peptide units composed of two Deg residues. Table 3 also clearly shows that the properties of the ester $\text{C}=\text{O}$ mode are not dependent on n . Its frequency and dipole derivative are about $1724\text{--}1725\text{ cm}^{-1}$ and $2.2\text{ D Å}^{-1}\text{ amu}^{-1/2}$, respectively.

A similar distinction is seen for the amide II local modes as well (Table 3). The frequencies and dipole derivatives are in the range of $1479\text{--}1480\text{ cm}^{-1}$ and $3.0\text{--}3.1\text{ D Å}^{-1}\text{ amu}^{-1/2}$ (the units at the N-terminus), $1486\text{--}1487\text{ cm}^{-1}$ and $3.4\text{--}3.6\text{ D Å}^{-1}\text{ amu}^{-1/2}$ (the middle units), and $1493\text{--}1495\text{ cm}^{-1}$ and $3.0\text{--}3.2\text{ D Å}^{-1}\text{ amu}^{-1/2}$ (the units at the C-terminus). The amide II frequency shift induced by hydrogen bonding is the opposite of that of the amide I,^{65,81} and hence, the units at the N-terminus, lacking of the C_5 hydrogen bond at the $\text{C}=\text{O}$ group, have lower frequencies than those of the other units.

Let us now consider the relative dipole derivatives between the amide I and II local modes. It is intriguing that the values of the amide I local modes are smaller compared to those of the amide II modes. The ratio of dipole derivatives ($\mu_{\text{I}}/\mu_{\text{II}}$) is about 0.9 for the N-terminal unit and 0.7–0.75 in the other units, regardless of the chain length. FT IR measurements of NMA obtained a dipole strength ratio of 1.41 between the amide I and II modes in acetonitrile⁶⁵ and 1.12 in H_2O .⁵⁷ A ratio of 1.19 was used to reproduce the measured 2D IR amide I/II spectra of $\text{NMA-}h_7$ in DMSO.⁴⁰ In our recent DFT calculation at the level of B3LYP/6-311++G(d,p), this ratio was 1.39 for NMA and decreased to 1.00 when the methyl groups of NMA were replaced with the *tert*-butyl groups,⁴⁷ indicating that substituents on the α -carbons can affect the local transition dipole ratio in the case of polypeptides. It is very difficult to prepare a fully extended polypeptide chain composed of protein amino acid residues and test the substitution effects experimentally due to their conformational flexibility. Therefore, we investigated this theoretically by repeating the same calculation for a capped glycine pentapeptide (GP), $\text{Ac-Gly}_5\text{-OtBu}$, in vacuo to check whether the IR properties calculated for the Deg peptides are induced by the ethyl side chains on the α -carbons or not. In this calculation for GP, the hydrogen atoms on C^α were included in the higher ONIOM layer. Table 3 lists the calculated local-mode properties. The frequencies and dipole derivatives of the amide I local modes are in the range of $1699\text{--}1704\text{ cm}^{-1}$ and $2.4\text{--}2.6\text{ D Å}^{-1}\text{ amu}^{-1/2}$, respectively. The three different types of peptide units cannot be clearly identified in GP. Compared to the calculation results for $\text{Ac}(\text{-Deg})_5\text{-OtBu}$, the frequencies become larger, especially for the second through fourth units, which are between two neighboring residues and hence most affected by the substitution effects at the α -carbons. The amide II local-mode frequencies also increase by $30\text{--}40\text{ cm}^{-1}$ for all of the peptide units. Their dipole derivatives decrease by 10–26%, leading to a ratio between the amide I and II modes of 1.1 for the N-terminal unit and 0.83–0.96, still lower than 1, for the other four units.

Figure 7 shows the scaled normal-mode frequencies and infrared intensities of $\text{Ac}(\text{-Deg})_n\text{-OtBu}$ ($n = 2\text{--}5$) as well as those of GP as stick spectra. Their values are listed in Table S1, Supporting Information. The ester $\text{C}=\text{O}$ stretching mode of the

Table 1. Average Dihedral Angles (in degrees) of Ac-(Deg)_n-OtBu Obtained from 15 ns MD Trajectories in CDCl₃ and of Tfa-(Deg)_n-OtBu Crystals Determined by X-ray Diffraction Analysis (*n* = 3 and 5)

residue ^a	Ac-(Deg) _n -OtBu ^b				Tfa-(Deg) _n -OtBu ^c			
	<i>n</i> = 3		<i>n</i> = 5		<i>n</i> = 3		<i>n</i> = 5	
	ϕ	ψ	ϕ	ψ	ϕ	ψ	ϕ	ψ
1	179.8(7.2)	179.8(10.6)	−179.9(7.2)	177.8(9.8)	180	180	179	171
2	−178.6(8.3)	177.7(10.3)	−179.3(7.1)	176.9(9.5)	180	180	176	−174
3	−178.2(7.3)	178.4(13.4)	−177.6(7.0)	−176.4(9.4)	180	180	−173	180
4			179.6(7.0)	−176.9(9.9)			179	170
5			177.7(7.1)	179.2(12.0)			175	−178

^aThe residues are numbered from the N- to C-terminus. ^bStandard deviations are denoted in parentheses. ^cReference 14. The average estimated standard deviations for bond angles are in the range of 0.5–3.5°.

Table 2. Structural Parameters of the C_S Intramolecular Hydrogen Bond in Ac-(Deg)_n-OtBu Obtained from 15 ns MD Trajectories in CDCl₃ and of Tfa-(Deg)_n-OtBu Crystals Determined by X-ray Diffraction Analysis (*n* = 3 and 5)

residue ^a	Ac-(Deg) _n -OtBu ^b						Tfa-(Deg) _n -OtBu ^c					
	<i>n</i> = 3			<i>n</i> = 5			<i>n</i> = 3			<i>n</i> = 5		
	N···O (Å)	H···O (Å)	∠NHO (degree)	N···O (Å)	H···O (Å)	∠NHO (degree)	N···O (Å)	H···O (Å)	∠NHO (degree)	N···O (Å)	H···O (Å)	∠NHO (degree)
1	2.66 (0.08)	2.16 (0.12)	108.6 (4.7)	2.66 (0.08)	2.17 (0.12)	108.4 (4.7)	2.52	1.98	111.5	2.56	2.06	114.8
2	2.62 (0.07)	2.08 (0.11)	110.7 (4.9)	2.62 (0.07)	2.09 (0.11)	110.4 (4.8)	2.57	2.06	108.6	2.55	2.07	112.5
3	2.65 (0.07)	2.15 (0.12)	108.9 (4.7)	2.65 (0.07)	2.15 (0.12)	109.2 (4.7)	2.58	2.05	109.1	2.55	2.07	113.1
4				2.62 (0.07)	2.09 (0.11)	110.5 (4.8)				2.57	2.11	112.1
5				2.66 (0.07)	2.15 (0.11)	108.9 (4.7)				2.55	2.11	110.9

^aThe residues are numbered from the N- to C-terminus. ^bStandard deviations are denoted in parentheses. ^cReference 14.

Deg peptides has a frequency of 1727–1728 cm^{−1}, shifted by 3 cm^{−1} from the local-mode frequency, and there is no noticeable change in the dipole derivatives. The trend of the amide I normal modes is a greater intensity at the lowest and highest frequencies, and their separation ($\Delta\tilde{\nu}_{\text{I,peak}}$) increases from 17 (*n* = 2) to 26 cm^{−1} (*n* = 5) as a function of the chain length as plotted in Figure 7b (red circles). The total IR intensity exhibits a monotonic increase in Figure 7c (red circles).

For the amide II modes, the lowest-frequency normal mode possesses a much larger IR intensity than any other mode (Figure 7a). Its frequencies ($\tilde{\nu}_{\text{II,peak}}$) decrease with *n* from 1479 to 1472 cm^{−1} (Figure 7b, blue circles). The relative intensity ratio between the strongest and second strongest normal modes is 4.7, 8.2, 10.3, 13.8 from *n* = 2 to 5. It is clear from Figure 7c (blue circles) that the total intensity significantly grows when increasing the length. As expected from the ratio of the local-mode intensities, the amide II normal modes also exhibit much larger intensities than the amide I normal modes for all chain lengths, and the $I_{\text{I}}/I_{\text{II}}$ ratio between the two decreases from 0.64 to 0.42 with increasing *n* (Figure 7c, black circles).

The normal-mode properties of the fully extended GP are similar to those of the Deg homopeptide, except for the overall frequencies, which are higher by 9–21 cm^{−1}. In Figure 7b

and c, $\Delta\tilde{\nu}_{\text{I,peak}}$, $\tilde{\nu}_{\text{II,peak}}$, and the total amide I and II intensities as well as their ratio are plotted. The intensity ratio is 0.59, higher than the value of Deg homopeptide but much lower than 1.

The nearest-neighbor couplings of the amide I/I ($\beta_{\text{I}-\text{I}}$), I/II ($\beta_{\text{I}-\text{II}}$), II/I ($\beta_{\text{II}-\text{I}}$), and II/II ($\beta_{\text{II}-\text{II}}$) were calculated by the finite energy difference method after acquiring the local-mode coordinates in each peptide unit.⁴⁷ In contrast to the local-mode frequencies and transition dipole derivatives, which are dependent on the different types of the peptide units shown in Figure 1, the couplings are almost independent of which types of peptide units constitute the neighbors, and their values are $\beta_{\text{I}-\text{I}} = 7.0 \text{ cm}^{-1}$, $\beta_{\text{I}-\text{II}} = -3.8 \text{ cm}^{-1}$, $\beta_{\text{II}-\text{I}} = -24 \text{ cm}^{-1}$, and $\beta_{\text{II}-\text{II}} = -3.0 \text{ cm}^{-1}$ (Table 5). The amide II/I coupling strength is quite large, most probably because the N–H and C=O groups in the two nearest-neighbor peptide units are on the same Deg residue and are forming the C_S intramolecular hydrogen bond. In the ideal fully extended structure, the transition charge couplings between the amide modes in non-nearest-neighbor units were estimated to be less than 1 cm^{−1}, and hence, the nearest-neighbor couplings affect the linear and 2D IR spectra to a much greater degree.

C. Model Calculation of Linear and 2D IR Spectra. An ideal fully extended polypeptide chain $[(\phi,\psi) = (\pm 180^\circ, \pm 180^\circ)]$ with *n* residues was built based on the average conformational

Table 3. Scaled Local Mode Frequencies (cm^{-1}) and Transition Dipole Derivatives ($\text{D Å}^{-1} \text{amu}^{-1/2}$) of the Fully Extended Ac-(Deg)_n-OtBu ($n = 2-5$) and Capped Glycine Pentapeptide (GP), Ac-Gly₅-OtBu, Calculated with the ONIOM (B3LYP/6-31+G(d) and AM1) Method in Vacuo, and the Best Parameters Extracted from Model Calculation of Linear and 2D IR Spectra

unit ^a	ONIOM calculation ^b					model spectral calculation				
	Ac-(Deg) _n -OtBu, n					GP	Ac-(Deg) _n -OtBu, n			
	2	3	4	5	GP		2	3	4	5
Ester C=O	1725(2.2)	1725(2.2)	1725(2.2)	1724(2.2)	1734(2.4)	1717(2.8)	1717(2.8)	1717(2.8)	1717(2.8)	1717(2.8)
Amide I										
1	1685(2.7)	1684(2.7)	1684(2.7)	1684(2.8)	1700(2.6)	1660(2.6)	1660(2.6)	1660(2.6)	1660(2.6)	1660(2.6)
2	1675(2.2)	1670(2.5)	1670(2.5)	1669(2.5)	1699(2.5)	1656(2.4)	1656(2.5)	1656(2.5)	1656(2.5)	1656(2.5)
3		1678(2.3)	1673(2.6)	1672(2.6)	1701(2.6)		1656(2.4)	1656(2.5)	1656(2.5)	1656(2.5)
4			1678(2.4)	1672(2.6)	1701(2.6)			1656(2.4)	1656(2.5)	1656(2.5)
5				1678(2.4)	1704(2.4)				1656(2.4)	1656(2.4)
Amide II										
1	1480(3.0)	1479(3.0)	1480(3.0)	1480(3.1)	1512(2.3)	1510(3.3)	1510(3.3)	1510(3.3)	1510(3.3)	1510(3.3)
2	1494(3.0)	1486(3.4)	1486(3.4)	1486(3.5)	1524(2.7)	1515(3.4)	1510(3.7)	1510(3.7)	1510(3.7)	1510(3.7)
3		1493(3.1)	1487(3.5)	1487(3.6)	1525(2.7)		1515(3.4)	1510(3.7)	1510(3.7)	1510(3.7)
4			1495(3.2)	1487(3.6)	1526(2.8)			1515(3.4)	1510(3.7)	1510(3.7)
5				1494(3.2)	1530(2.9)				1515(3.4)	1515(3.4)

^a The peptide units are numbered from the N- to C-terminus. ^b A frequency scaling factor of 0.9774 was used for the ester C=O stretching and the amide I modes, and 0.9665 was used for the amide II modes.⁸³ Transition dipole derivatives are shown in parentheses.

parameters of the Deg residue.¹⁴ In the calculation, we started with the vibrational properties obtained in the previous subsection and slightly adjusted some of the parameters in order to reproduce the measured linear and 2D IR spectra. The best set of local frequencies and dipole strengths extracted from this model calculation are summarized in Table 3. The amide I/II coupling in the same peptide unit was set to -27 cm^{-1} , the experimentally determined value for NMA,³⁹ and the nearest-neighbor couplings were finally set to the following values: $\beta_{\text{I}-\text{I}} = 4.3 \text{ cm}^{-1}$, $\beta_{\text{I}-\text{II}} = -3.8 \text{ cm}^{-1}$, $\beta_{\text{II}-\text{I}} = -24 \text{ cm}^{-1}$, and $\beta_{\text{II}-\text{II}} = -3.5 \text{ cm}^{-1}$. The signs of amide I/II and amide II/I couplings were set following the same procedure as discussed in the previous study.⁴⁷ Local transition dipoles of the amide I and ester C=O modes were orientated 11 and 8° away from the C=O bond, and that of the amide II was set to 87° away from the N-H bond based on the ONIOM calculation results on the capped Deg homopeptides. To take into account the inhomogeneous frequency distribution, mainly due to the fluctuations in the C₅ intramolecular hydrogen bond, Gaussian distributions with standard deviations of 8.0 and 7.5 cm^{-1} around the mean frequencies of the amide I and II modes were assumed, and 7500 different sets of frequencies were utilized to calculate linear and 2D IR spectra with a homogeneous line width of 12 cm^{-1} (FWHM). It has been previously shown that the 2D IR spectral shapes are more sensitive to the frequency fluctuations rather than those of coupling strengths.⁸⁴

A two-exciton Hamiltonian was built from the one-exciton Hamiltonian with harmonic approximation. The diagonal anharmonicities of the amide I and II modes were set to 16^{51} and 10 cm^{-1} ,⁴⁰ respectively. The Hamiltonians were diagonalized to obtain the transition frequencies and dipole strengths of the exciton states. The formulas to compute linear and 2D IR spectra for $\langle Y, Y, Z, Z \rangle$ and $\langle \pi/4, -\pi/4, Y, Z \rangle$ in the R pulse sequence have been described previously.^{36,71,85} The following equations³⁸

were used for the NR 2D spectra under $\langle \pi/4, Y, -\pi/4, Z \rangle$

$$S_{\text{NR}}(\omega_\tau, \omega_t; T = 0) = S_{\text{b-a-c}}(\omega_\tau, \omega_t) + S_{\text{b-c-a}}(\omega_\tau, \omega_t) \quad (1)$$

$$S_{\text{b-a-c}}(\omega_\tau, \omega_t) = \left\langle \sum_{i,j} \frac{1}{i(\omega_\tau - \omega_i) - \gamma} \left[\frac{O_{i,j}^4}{i(\omega_t - \omega_j) - \gamma} \right. \right. \\ \left. \left. + \frac{O_{i,j}^5}{i(\omega_t - \omega_i) - \gamma} - \sum_k \frac{O_{i,j,k}^6}{i(\omega_t - \omega_{kj}) - \gamma} \right] \right\rangle \quad (2)$$

$$S_{\text{b-c-a}}(\omega_\tau, \omega_t) = \left\langle \sum_{i,j,k} \frac{1}{i(\omega_\tau - \omega_i) - \gamma} \left[\frac{O_{i,j,k}^7}{i(\omega_t - \omega_j) - \gamma} \right. \right. \\ \left. \left. - \frac{O_{i,j,k}^8}{i(\omega_t - \omega_{kj}) - \gamma} \right] \right\rangle \quad (3)$$

Here, i and j represent the one-exciton states, and k represents the two-exciton states. The transition frequencies between the ground and one-exciton states and between the one- and two-exciton states are represented by $\omega_{i(j)}$ and $\omega_{k(i(j))} = \omega_k - \omega_{i(j)}$, respectively. The homogeneous line width (HWHM) γ was set to 6 cm^{-1} . The orientation factors, O^n , are summarized in Table 4. This polarization configuration suppresses the diagonal peaks because $O^4 = O^7 = 0$ when $i = j$. The suppression is complete in the harmonic and extremely weak coupling case where $\mu_{ik} = 2^{1/2} \mu_i$ (here, k denotes the overtone state), and thus, $O^6 = O^8 = 0$. The set of cross-peaks in the diagonal region is suppressed because $O^5 = 0$, whereas the other set of cross-peaks in the off-diagonal regions survives if the angles between the excitonic transition dipoles are not 0. Therefore, the NR spectra will only contain off-diagonal features. This behavior is different

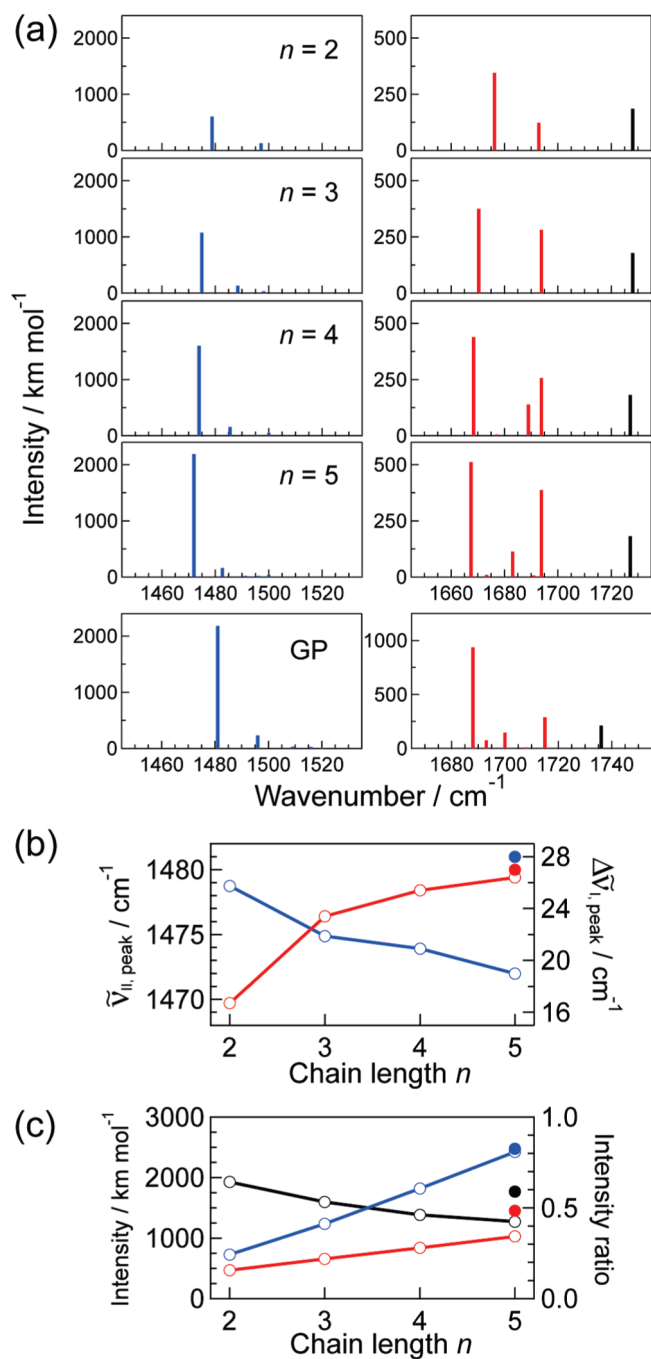


Figure 7. (a) Stick spectra of the normal modes calculated for the fully extended $\text{Ac}(\text{Deg})_n\text{-OtBu}$ ($n = 2-5$) peptides and capped Gly pentapeptide (GP), $\text{Ac-Gly}_5\text{-OtBu}$, with the ONIOM (B3LYP/6-31+G(d)/AM1) method: the amide I (red); the amide II (blue); the ester C=O stretching (black). (b) Differences between the lowest and highest amide I normal-mode frequencies, $\Delta\tilde{\nu}_{I,\text{peak}}$ (red, open circles) and the peak position of the lowest-frequency amide II normal mode $\tilde{\nu}_{II,\text{peak}}$ (blue, open circles) of $\text{Ac}(\text{Deg})_n\text{-OtBu}$. (c) The total IR intensities of the amide I (red, open circles), amide II (blue, open circles), and their ratio I_I/I_{II} (black, open circles) of $\text{Ac}(\text{Deg})_n\text{-OtBu}$. The corresponding values of GP are also plotted as closed circles in panels (b) and (c).

from those of NR cross-peak patterns obtained using $\langle \pi/4, -\pi/4, Y, Z \rangle$, which are along the diagonal.^{37,38}

The simulated linear spectra are superimposed on the measurement results in Figure 2a (dashed lines), after normalization

by the peak intensity of the ester C=O mode. The frequency separation between the two amide I peaks ($\Delta\tilde{\nu}_{I,\text{peak}}$, red squares) and the peak frequency of the amide II mode ($\tilde{\nu}_{II,\text{peak}}$, blue squares) are plotted in Figure 2b. The calculation results agree with the measurements within a few cm^{-1} . The integrated intensities of the amide I (red squares) and the amide II (blue squares) and their ratio (black squares) are compared with those from the measured spectra in Figure 2c. The deviations in intensities are less than 20%. The observed trends, that is, the monotonic intensity increase with the chain length and the I_I/I_{II} ratio being less than 1, are reproduced well.

In the right columns of Figures 3–6, the simulated 2D IR cross-peak patterns of the amide I modes and the amide I/II 2D spectra are arranged for comparisons to the measurement. Overall, we achieve good agreement between the measured and calculated spectra for the R and NR pulse sequences as well as those under different polarization configurations. On the basis of the agreement, we conclude that the capped Deg homopeptides in CDCl_3 took the fully extended C_S conformation from dipeptide to pentapeptide. This determination of peptide backbone conformation was indirectly speculated in the previous ^1H NMR and FT IR measurements of the N–H groups,¹⁵ but 2D IR spectroscopy now provides much more direct evidence. The agreement between experiment and calculation are better for the longer peptides than that for the dipeptide, suggesting that the dipeptide may be more flexible in its structure.

D. Excitonic Properties of a Fully Extended Polypeptide Chain. We investigated the excitonic properties of vibrational modes in a fully extended polypeptide chain in a general way and applied a theoretical analysis to the amide I and II modes. As pointed out earlier, the transition charge couplings among the amide modes in non-nearest peptide units are much smaller than those in the nearest-neighbor couplings. As a first approximation, therefore, the non-nearest-neighbor couplings are set to 0 in the exciton Hamiltonian, which leads to a tridiagonal matrix form as follows

$$\begin{bmatrix} \varepsilon_1 & \beta_{12} & & & \\ \beta_{21} & \varepsilon_2 & \beta_{23} & & \\ \beta_{32} & & \varepsilon_3 & \ddots & \\ & & & \ddots & \\ & & & & \varepsilon_{N-2} & \beta_{N-2N-1} \\ & & & & \beta_{N-1N-2} & \varepsilon_{N-1} & \beta_{N-1N} \\ & & & & & \beta_{NN-1} & \varepsilon_N \end{bmatrix} = \begin{bmatrix} \varepsilon & \beta & & & \\ \beta & \varepsilon & \beta & & \\ \beta & & \varepsilon & \ddots & \\ & & & \ddots & \\ & & & & \varepsilon & \beta \\ & & & & \beta & \varepsilon & \beta \\ & & & & & \beta & \varepsilon \end{bmatrix} \quad (4)$$

Here, for simplicity, the local energy (ε_i) and the nearest-neighbor couplings (β_{ij}) are assumed constant and set to ε and β , respectively; N is the number of peptide units in a chain. Diagonalization of this Hamiltonian resulted in the energies (λ_m) and squared transition dipole strengths ($|\mu_m|^2$) of m

exciton states ($m = 1, \dots, N$)

$$\lambda_m = \varepsilon + 2\beta \cos \frac{m\pi}{N+1} \quad (5)$$

$$|\boldsymbol{\mu}_m|^2 = (Q_o^2 + 2Q_o Q_e \cos \theta_{oe} + Q_e^2) |\boldsymbol{\mu}^0|^2 \quad (6)$$

$$Q_o = \left(\frac{2}{m+1} \right)^{1/2} \sum_{m'} \sin \frac{(2m'-1)m\pi}{N+1}$$

$$Q_e = \left(\frac{2}{m+1} \right)^{1/2} \sum_{m'} \sin \frac{2m'm\pi}{N+1} \quad 1 \leq m' \leq N/2 \quad (7)$$

In eq 6, $|\boldsymbol{\mu}^0|$ is the magnitude of the local transition dipole moment. Here, we have assumed that the local transition dipole angles are parallel to one another on every other peptide unit but are alternating between the nearest-neighbor peptide units with the angle θ_{oe} (see, e.g., the amide I modes in Figure 8c). The above equations are quite general, applicable to any θ_{oe} , whereas equations from previous studies were derived only for the case of all molecules arranged in parallel ($\theta_{oe} = 0^\circ$).^{86,87} Note that the coupling strength β affects only the exciton state energies λ_m , and that θ_{oe} is the sole parameter in determining the transition strength.

Figure 8a depicts the resulting features for a fully extended linear chain with 50 peptide units. As expected from eq 5, the

exciton state energies λ_m have a cosine dependence on the quantum number m and is independent of θ_{oe} . If the coupling is positive in sign, the lowest quantum number m state is the highest in energy, whereas the highest m state has the lowest energy (red). Changing the sign of the coupling reverses the energy order (blue). It is clear from this very long chain case that θ_{oe} drastically alters the intensities of exciton transitions. If all of the local dipoles point to the same direction ($\theta_{oe} = 0^\circ$, left) over the entire chain, the exciton state with the lowest quantum number m acquires nearly all of the transition strength regardless of the sign of the coupling. Thus, transition to the highest (lowest)-energy exciton state is the strongest for a positive (negative) coupling. If the local dipoles alternately reverse their directions ($\theta_{oe} = 180^\circ$, right), the opposite trend is observed with the highest m state acquiring most of the transition strength. If two nearest-neighbor local transition dipoles are oriented perpendicularly with each other ($\theta_{oe} = 90^\circ$, middle), the two exciton states with the lowest and highest energies are equally intense and much stronger than any other states. Only some exciton states whose energies are close to the minimum or maximum exhibit noticeable strengths.

The chain length dependence ($N = 2-5$) of the exciton properties are presented in Figure 8b for $\beta = \pm 5 \text{ cm}^{-1}$ and $\theta_{oe} = 90^\circ$. We can notice effects of the finite unit number in eqs 5–7 on both $\lambda_m - \varepsilon$ and $|\boldsymbol{\mu}_m|^2$. The absolute energy differences of the lowest and highest states are 10 cm^{-1} for $N = 2$, increasing up to 17.3 cm^{-1} for $N = 5$, which is still slightly lower than the limiting value of 20 cm^{-1} for an infinitely long chain. The lowest- and highest-energy states always have equally large transition strengths even for these short chains, and their magnitudes become larger with N . Compared to these two states, other states have almost zero or just tiny strengths, as in an ideally long chain.

It will be of interest to apply the parameters used in the model calculation of the amide I and II modes, even though the theoretical treatment of the linear exciton chain cannot apply to two sets of different local modes coupled with each other. Figure 8c illustrates a pentapeptide chain in a stick representation as well as the transition dipole directions of the local amide I (red)

Table 4. Orientation Factors for the Polarization $\langle \pi/4, Y, -\pi/4, Z \rangle$ Configuration in the NR Pulse Sequence

	pulse sequence	orientation factor
b-a-c	O_{ij}^4	$- \boldsymbol{\mu}_i ^2 \boldsymbol{\mu}_j ^2 + (\boldsymbol{\mu}_i \cdot \boldsymbol{\mu}_j)^2$
	O_{ij}^5	0
	$O_{ij,k}^6$	$-(\boldsymbol{\mu}_i \cdot \boldsymbol{\mu}_j)(\boldsymbol{\mu}_{ik} \cdot \boldsymbol{\mu}_{kj}) + (\boldsymbol{\mu}_i \cdot \boldsymbol{\mu}_{ik})(\boldsymbol{\mu}_j \cdot \boldsymbol{\mu}_{jk})$
b-c-a	O_{ijk}^7	$-(\boldsymbol{\mu}_i \cdot \boldsymbol{\mu}_{jk})(\boldsymbol{\mu}_j \cdot \boldsymbol{\mu}_{ij}) + (\boldsymbol{\mu}_i \cdot \boldsymbol{\mu}_{ik})(\boldsymbol{\mu}_j \cdot \boldsymbol{\mu}_{jk})$
	$O_{ij,k}^8$	$-(\boldsymbol{\mu}_i \cdot \boldsymbol{\mu}_j)(\boldsymbol{\mu}_{ik} \cdot \boldsymbol{\mu}_{kj}) + (\boldsymbol{\mu}_i \cdot \boldsymbol{\mu}_{ik})(\boldsymbol{\mu}_j \cdot \boldsymbol{\mu}_{jk})$

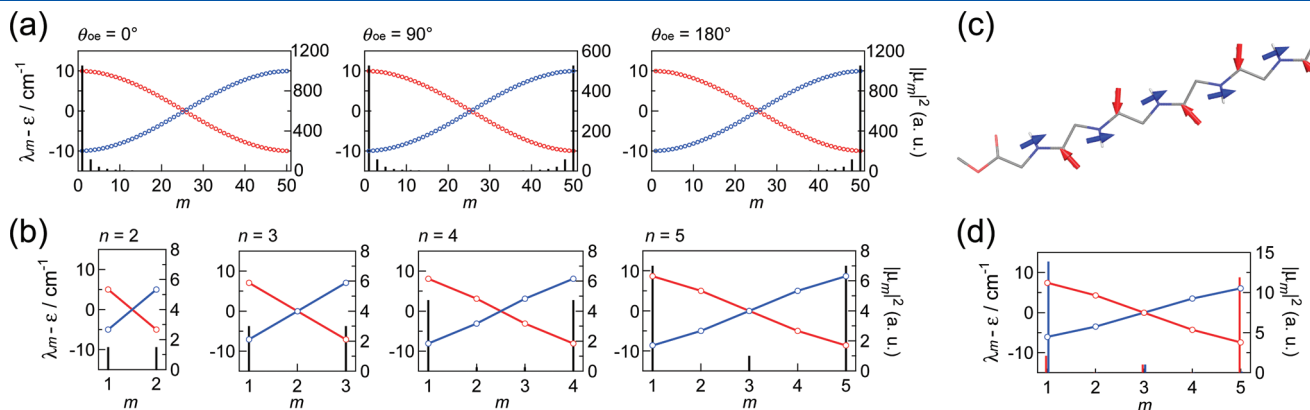


Figure 8. Excitonic properties calculated for the fully extended structure with $(\phi, \psi) = (\pm 180^\circ, \pm 180^\circ)$. (a) Differences of energy in exciton and local states (circles, left axis) and squared transition dipole strengths (black sticks, right axis) of the exciton state m for the nearest-neighbor coupling of 5 cm^{-1} (red circles) and -5 cm^{-1} (blue circles); angle between the nearest-neighbor dipoles of the local modes, $\theta_{oe} = 0^\circ$ (left), $\theta_{oe} = 90^\circ$ (middle), $\theta_{oe} = 180^\circ$ (right). (b) Exciton properties for the fully extended polypeptide chain with n ($n = 2-5$) residues. The coupling strength is 5 cm^{-1} (red) and -5 cm^{-1} (blue), and θ_{oe} is set to 90° . Lines through the circles are drawn as a guide for the eyes. (c) Transition dipole configuration of the local amide I (red) and amide II (blue) modes in the ideal fully extended pentapeptide used in the model calculation. Atoms in the side chain groups are omitted in the stick representation of the peptide backbone. (d) Excitonic properties of the amide I (red) and amide II (blue) modes calculated for the pentapeptide configuration shown in (c) with the nearest-neighbor couplings set to the values used in the model spectral calculation.

arrows) and amide II (blue arrows) modes on the peptide units. The angle θ_{oe} of 135° (7°) and the nearest-neighbor coupling strength of 4.3 cm^{-1} (-3.5 cm^{-1}) were substituted into eqs 5–7 to evaluate the exciton properties for the amide I (II) modes and plotted in red (blue) in Figure 8d. Both amide I and II excitons exhibit roughly a large transition at the low-frequency end of the band, but the underlying causes are not the same for the two cases. The amide I modes interact with a positive coupling and the nearest-neighbor dipole angle in the range of $90 < \theta_{oe} < 180^\circ$. In contrast, a combination of the negative coupling and the dipole angle close to 0° is the reason that the lowest amide II exciton state gains the largest transition strength. These comparisons indicate that the band shapes experimentally observed in linear spectra would not allow us to unambiguously determine the molecular parameters such as β and θ_{oe} . Another important fact is that the amide I and II modes are coupled and not fully isolated from one another.^{39–41,44,45,47,49} The theoretical features in Figure 8d reproduce those of the observed amide I and II bands in Figure 2a, except that the relative intensity of the calculated $m = 1$ amide I exciton state should have been stronger in order to better match that of the measured high-frequency amide I band. This deficiency is mainly because the couplings between the amide I and II modes in the intra- and interpeptide units are completely ignored in the linear exciton analysis summarized in eqs 5–7.

V. DISCUSSION

A. Molecular Conformation and Flexibility of Deg Homopeptides in CDCl_3 . We obtained a fine agreement between the experiment and simulation of the amide I/II linear (Figure 2) and 2D IR (Figures 3–6) spectra. It verifies that the Ac-capped Deg homopeptides adopt the fully extended conformation as assumed in our model calculation and that the parameters evaluated from ONIOM calculations are approximately correct. In the peptide structure directly determined by 2D IR spectroscopy, all of the N–H groups form intramolecular C_5 hydrogen bonds, and are inaccessible to solvent molecules to form intermolecular hydrogen bonds. This is consistent with the experimental results of ^1H NMR titration by DMSO and TEMPO in the previous works.^{15,19} The extended conformation exists in solution even at the dipeptide level.

Fluctuations of the fully extended conformation provide valuable information on the rigidity of the Deg homopeptides. The standard deviations of ϕ (σ_ϕ) and ψ (σ_ψ) are $7.0–7.2$ and $9.4–12.0^\circ$, respectively, for the fully extended pentapeptide in the MD simulation. An Aib-rich 3_{10} -helical hexapeptide Z-Aib-L-Leu-(Aib)₂-Gly-Aib-OtBu (Z, benzyloxycarbonyl, abbreviated as Z6 hereafter) in CDCl_3 fluctuates with σ_ϕ in the range of $7.3–14.8^\circ$ and with σ_ψ in the range of $8.9–17.0^\circ$, as simulated by the same AMBER ff 99SB force field.⁴⁸ The wider ranges of fluctuations in the Z6 peptide are due to the flexible Gly residue near the C-terminus; the fluctuations around the three N-terminal and central Aib residues are comparable with those of the Deg homopentapeptide ($\sigma_\phi = 7.7–8.7^\circ$; $\sigma_\psi = 9.2–10.3^\circ$). In another study of the 3_{10} -helical Z-[L-(α Me)Val]₈-OtBu [(α Me)Val, C $^\alpha$ -methylvaline] peptide in CDCl_3 , the measured 2D IR spectra were well reproduced by a restrained simulation under the CHARMM 22 force field and exhibited fluctuations of $5.0–6.0^\circ$ for both of ϕ and ψ .³⁸ These MD results indicate that the magnitude of backbone fluctuations for C $^\alpha,\alpha$ -dialkylated residues in short peptides is similar, and the length of the alkyl side chains

Table 5. Nearest-Neighbor Couplings^a between the Amide I/I, I/II, II/I, and II/II Modes Calculated for *N*-Acetylglycine-N'-methylamide with $(\phi,\psi) = (\pm 180^\circ, \pm 180^\circ)$ and Calculated and Experimentally Determined for Deg Homopeptides

map	method ^b	ref	I/I	I/II	II/I	II/II
Torii	HF/6-31+G(d,p) FED	52	4.1			
Cho	HF/6-311++G(d,p) HMR	54	6.5			
Stock	B3LYP/6-31G+(d) HMR	58	8.4			
Knoester	RPBE/TZ2P HMR	59	6.3			
Mukamel	BPW91/6-31G(d,p) PE	61	6.5	c	21	0.8
Ge	B3LYP/6-31G+(d) FED	47	6.7	-2.7	-14	-0.4
ONIOM	B3LYP/6-31G+(d)/AM1	this study	7.0	-3.8	-24	-3.0
	FED					
exp.	spectral calculation	this study	4.3	-3.8	-24	-3.5

^aThe units of the couplings were converted from $\text{mdyn \AA}^{-1} \text{amu}^{-1}$ to cm^{-1} with the local amide I and II mode frequencies of 1650 and 1500 cm^{-1} , respectively. ^bThe functional and basis set used in quantum mechanical calculation are indicated in the upper line. Nearest-neighbor couplings were calculated using the method indicated in the lower line; FED, finite energy difference method; HMR, Hessian matrix reconstruction; PE, potential expansion to fourth order in the local amide modes.

^cThis coupling map is not available.

does not have strong effects on the backbone stability. As discussed in the following subsection, we have to consider a way to correlate the conformational fluctuations with the frequency distribution of the amide modes.

B. Vibrational Couplings and Frequency Distributions in the Deg Homopeptides. In the model calculation, we estimated the initial values of the nearest-neighbor coupling strengths from the ONIOM calculations. Although many coupling^{44,47,52,54,58,59} maps have been created based on quantum mechanical calculations of a model peptide, Ac-Gly-NHMe, it is still not clear which maps are best for building the vibrational exciton Hamiltonian. This situation can be mainly attributed to the lack of test molecules with well-defined conformations. However, the Deg residue in the homopeptides has a propensity toward the fully extended conformation with $(\phi,\psi) \approx (\pm 180^\circ, \pm 180^\circ)$, making it ideal for comparisons between experiments and calculations. Table 5 summarizes the nearest-neighbor coupling strengths of the amide I/I, I/II, II/I, and II/II modes evaluated at $(\phi,\psi) = (\pm 180^\circ, \pm 180^\circ)$ from available maps.^{44,47,52,54,58,59} The amide I/I coupling determined in this study (4.3 cm^{-1}) is closer to the value in the Torii's map (4.1 cm^{-1}) rather than the others, which are in the range of $6.3–8.4 \text{ cm}^{-1}$. Only a few maps have been created for the amide I/II, II/I and II/II coupling strengths thus far.^{44,47,52,54,58,59} Our previous coupling maps⁴⁷ underestimated the magnitudes, especially for the amide II/I and amide II/II. The latter is a main factor causing the red shift of the $\tilde{\nu}_{\text{II,peak}}$ in the linear IR spectra (Figure 2b, blue), and the value from our map (-0.4 cm^{-1}) was unable to replicate it at all. A similarly small amide II/II coupling strength was obtained by Hayashi and Mukamel.⁴⁴ The magnitude of their amide II/I coupling was close to that determined in this study.

Let us compare frequency distributions of the local amide I and II modes to those of the 3_{10} -helix. In our previous study of the 3_{10} -helical Aib homopeptides, $Z\text{-}(\text{Aib})_n\text{-OtBu}$ ($n = 3, 5, 8$, and 10), we employed a semiempirical model, which correlated the $\text{C=O}\cdots\text{H-N}$ inter-residue hydrogen bond electrostatic energies with the frequency shifts of the amide I modes.⁷¹ A series of linear and 2D IR measurements were well simulated by the model calculation, which included $8.5\text{--}11.0\text{ cm}^{-1}$ of the inhomogeneous frequency distributions originating from fluctuations of 3_{10} -helical hydrogen bonds between the i and $(i+3)$ th residues in the fluctuating peptide backbone with σ_ϕ and σ_ψ of $8.5\text{--}9.5^\circ$. The same model was also used for the 3_{10} -helical Z6 peptide, and the distributions of the amide I and II modes were $8.6\text{--}11.8$ and $11.9\text{--}13.8\text{ cm}^{-1}$, respectively.⁴⁷ Because this simple model has been quite successful in the simulation of 3_{10} -helices, we tried to convert the C_5 intramolecular hydrogen bond energies to the frequency shifts based on the same model in this study. However, the average frequency shifts were overestimated in the peptide units, with both the C=O and N-H groups being hydrogen bonded. Especially large were the blue shifts of the amide II modes ($36\text{--}37\text{ cm}^{-1}$), and if they were added to the gas-phase value of 1499 cm^{-1} ,⁶⁵ the simulated linear and 2D IR spectra were quite different from the measurements. The semiempirical model obtained the conversion factors by comparing the ab initio amide I and II frequencies of NMA-D₂O complexes as a function of the NMA-water distance.⁸¹ The failure of this model in simulating the C_5 conformation suggests that the through-bond effects may be important, similar to the case in which the transition dipole interaction is not able to approximate adequately the nearest-neighbor coupling strength.⁵³ Because this model was not applicable here, we set the inhomogeneity of the local amide I and II modes to 8.0 and 7.5 cm^{-1} , respectively, in the calculation to reproduce the experimental results of the Deg homopeptides. These values were smaller than those of the 3_{10} -helical peptides. Although σ_ϕ and σ_ψ around the Aib and Deg residues are very similar, the intraresidue C_5 hydrogen bond is expected to fluctuate less than the C_{10} hydrogen bond between the i and $(i+3)$ th residues that involves more pairs of dihedral angles. This led to narrower distributions of the amide I and II frequencies in the Deg homopeptides.

Different frequency maps assisted in correlating the frequency shift of the amide I^{55,56,60} and the amide II^{41,48,57,88} modes with electrostatic properties. Combining these maps with MD simulation trajectories worked quite well for simulating the 2D IR spectra of 3_{10} -helical peptides.^{38,48} A previous comparative study concluded that our electrostatic-potential-based model was capable of reproducing both of the amide I and II spectral features of the Aib-rich hexapeptides.⁴⁸ However, we noticed a problem when applying this map to the peptide units of the fully extended C_5 conformation. In the frequency calculation of the amide modes in a certain peptide unit, electrostatic potentials generated from atoms within the chromophore (a group of atoms that contains the parametrized atoms and has a zero net charge) needed to be excluded.^{38,84,89} In AMBER force fields, the definitions of the partial charges on atoms are such that each amino acid residue, including side chain atoms, is a charge-neutral group.⁷⁴ This meant that the charge neutrality requirement forced us to remove all of the atoms in the two Deg residues on both sides of the unit, including the C=O and N-H groups involved in the C_5 intramolecular hydrogen bonding. Because the frequency shifts of the amide I and II modes are most affected

by hydrogen bonding, the exclusion of these atoms rendered us unable to adequately evaluate the frequency distribution of each local mode. Therefore, we did not use a combination of the MD trajectory and the frequency map in this study, even though it had worked for the 3_{10} -helical peptides.⁴⁸

C. Amide I/II Spectral Features in the Fully Extended C_5 Conformation. After a thorough structure determination based on linear and 2D IR spectra, it is intriguing to discuss amide I and II spectral features observed for $\text{Ac}\text{-}(\text{Deg})_n\text{-OtBu}$ ($n = 2\text{--}5$) and the excitonic properties of the fully extended peptide chain. The amide I band exhibits two peaks in the FT IR spectra very clearly. This feature is quite distinct from the typical line shape of other conformations. For example, the α - and 3_{10} -helices typically show a single band peaked at $1648\text{--}1658$ and $1600\text{--}1666\text{ cm}^{-1}$, respectively.²⁸ The antiparallel β -sheet structure exhibits two amide I peaks, one at $\sim 1630\text{ cm}^{-1}$ and the other at $\sim 1680\text{ cm}^{-1}$,²⁸ and the frequency separation between the two ($\sim 50\text{ cm}^{-1}$) is about two times larger than that of the fully extended conformation ($\sim 29\text{ cm}^{-1}$ for $n = 5$). The 2D IR R cross-peak patterns shown in Figure 3 contain only two off-diagonal peaks in the amide I frequency region. The spectral pattern of 3_{10} -helical peptide with the same length, $Z\text{-}(\text{Aib})_5\text{-OtBu}$, is a doublet with a clear trench between the two peaks, which is distinguishable from the pattern of the C_5 conformation. The chain length dependence of R and NR cross-peak patterns indicates that three peptide units ($n = 3$) are required for the amide I spectra to converge and possess the characteristic pattern. In the case of the 3_{10} -helix, we experimentally found that the 2D IR spectra start convergence at the chain length with four peptide units.⁷¹ The fully extended C_5 conformation develops into a 2.0_5 -helix, and therefore, one may plausibly deduce a convergence length of the 2D IR spectral signatures as described by $l + 1$ peptide units for the helical conformations with the number of residues per turn, l .

The amide II band also exhibits traits characteristic of the fully extended conformation. The peak frequency of the band in the FT IR spectra (Figure 2), as well as that of the strongest diagonal band in the 2D IR spectra (Figures 5 and 6), decreases as the chain grows longer. This trend is consistent with the excitonic properties predicted from the analytic modeling. In contrast, the capped Aib homopeptides forming the 3_{10} -helix in CDCl₃ show a different chain length dependence of the amide II bands in linear IR spectra.⁴⁶ Only a single band appears at $\sim 1500\text{ cm}^{-1}$ for the shortest chain, and a new band grows in along with a blue shift of the peak position as the number of 3_{10} -helical turns increases. We assigned the lower- and higher-frequency bands to the amide II modes free from and involved in the 3_{10} -helical $\text{C=O}\cdots\text{H-N}$ hydrogen bonds, respectively, based on the tendency that hydrogen bonding on the peptide unit increases the frequency of the amide II mode. The comparisons of the chain length dependence in two different structures result in an important conclusion. The inter-residue hydrogen bonds indeed affect the local amide II frequency, but it is not the sole factor that determines the shape and peak position of the excitonic band observed in FT IR and 2D IR spectra. In the fully extended conformation, the number of peptide units whose C=O and N-H groups are involved in the intramolecular C_5 hydrogen bonding increases with the length. One may thus expect that the band would blue shift, as seen in the case of the 3_{10} -helix. However, the amide II band of the Deg homopeptides shows a red shift with the length (Figure 2b). As theoretically derived in section IV.D, the two molecular parameters, the nearest-neighbor couplings and the transition dipole angle, have to be taken

into account to properly predict the spectral profiles of the fully extended conformation. In other structures, the non-nearest-neighbor couplings are not necessarily negligible, and hence, they need to be included in the exciton Hamiltonian.

A brief comparison of the amide I/II 2D IR spectra between the 3_{10} -helical and fully extended peptides is worthwhile as well. The distinct linear spectra of the two conformations indicate that the amide I/II 2D IR patterns should also be different. This is indeed the case when compared to Z6 in CDCl_3 .⁴⁷ Its amide I diagonal band exhibited a single peak in the absolute magnitude R spectrum and also a slight hint of a high-frequency shoulder in the NR spectrum, and hence, almost no cross-peaks between the amide I modes were observed. The amide II band exhibits two diagonal peaks and two cross-peaks. Moreover, two cross-peaks between the amide I and II modes were observed above the diagonal line. These features are quite different from those in Figures 5 and 6. The spectral features in FT IR spectra may be enough to qualitatively determine peptide secondary structures and analyze their contents.^{26–28} However, it should be emphasized that only 2D IR spectroscopy can probe vibrational coupling strengths, important clues facilitating more detailed conformational analysis. Measurement and simulation of 2D IR amide I/II spectra are an epoch-making way in structure determination of biological molecules.

Finally, we discuss the total integrated intensity of the amide I and II bands. As many IR studies have shown, typically, the transition dipole strength, and hence the integrated intensity area, of the amide I is larger than that of the amide II.^{26,40,41,57,64–66} For example, proteins such as albumin, β -lactoglobulin, and myoglobin in aqueous solution showed the $I_{\text{I}}/I_{\text{II}}$ intensity ratio of about 2 when their linear IR spectra were measured in transmission mode.^{64,66} Interestingly, the attenuated total reflection measurement resulted in a reversed ratio of about 0.8 for albumin,⁶⁶ and the differences were ascribed to interface effects, which do not exist in our case. Another example is that an intensity ratio of about 1.3 was observed for 3_{10} -helical Z-(Aib)₁₀-OtBu in CDCl_3 .⁷¹ In contrast, the Deg homopeptides in CDCl_3 give a larger intensity to the amide II than the amide I, as shown in the transmission IR spectra (Figure 2c) and ONIOM calculations (Figure 7 and Table S1, Supporting Information). Furthermore, this is also the case for the magnitude of the local amide I and II dipole derivatives (Table 3). Considering the same trend obtained for the fully extended GP with $(\phi,\psi) = (\pm 180^\circ, \pm 180^\circ)$, the larger amide II intensity is unrelated to the substitution effects on the α -carbon atoms. From a DFT calculation at the B3LYP/D95(d,p) level, Kobko and Dannenberg also reported a similar reversal of the IR intensity for a polyglycine decapeptide forming an extended single β -strand.⁹⁰ Our further calculation of the fully extended Ac-(Deg)₅-OtBu, in which all of the hydrogen atoms of the alkyl groups were replaced with deuterium atoms, resulted in similar IR properties to those shown in Figure 7, and the ratio of the total infrared intensity was 0.38, quite close to the 0.42 of the undeuterated pentapeptide. This means that the methylene/methyl deformation modes do not have much influence on the amide I/II intensity reversal. Cheam and Krimm calculated vibrational properties of Ac-Gly-NHMe in the C_5 and C_7 conformations and predicted the reversed intensity ratio, which was contrary to their expectation.⁶³ We are certain that the Deg homopeptides take the C_5 conformation in CDCl_3 , and hence, our measurement and calculations of the reversed intensity ratio between the amide I and II modes are trustworthy. One may conclude that the

integrated intensity is not always larger for the amide I than the amide II mode, as shown in the case of the fully extended C_5 conformation.

VI. CONCLUDING REMARKS

We have measured the linear and 2D IR spectral signatures of the amide I and II modes of the $\text{Ac}(\text{Deg})_n\text{-OtBu}$ ($n = 2–5$) homopeptides in CDCl_3 in a combination of two pulse sequences with $\langle \pi/4, -\pi/4, Y, Z \rangle$, $\langle \pi/4, Y, -\pi/4, Z \rangle$, and $\langle Y, Y, Z, Z \rangle$ polarization configurations. On the basis of substantial agreement between spectral simulations and measurements, we determined their solution structure to be the fully extended C_5 conformation, which was indirectly speculated by ^1H NMR titration measurements thus far. Our conclusions are more direct because 2D IR spectral patterns are sensitive to the peptide conformation itself through coupling strengths and transition dipole angles between vibrational modes. The spectral profiles of both the amide I and II modes are quite different from those observed, for example, for 3_{10} -helical peptides in the same solvent, and they start to converge at $n = 3$.

A comprehensive analysis of the amide I and II modes in the fully extended C_5 structure was performed for the first time to our knowledge, partially because this conformation is hardly observable in peptides and proteins composed of protein amino acids. The well-restrained conformational character of the Deg residues makes it very useful for the novel design of functional motifs when it is desirable to have peptide units regularly aligned in a linear fashion. The analytic modeling of the linear exciton chain reasonably predicted the features of the amide I and II bands but less quantitatively for the amide I band. This was most likely due to the presence of vibrational couplings between the amide I and II modes in the same and next-neighbor peptide units, which were excluded in the simplified modeling. When both modes were included in the exciton Hamiltonian with coupling strengths very close to the values predicted from ONIOM calculations, the linear and 2D IR spectra for the resultant exciton states were very similar to those in measurements. Finally, it should be noted that the integrated amide II band intensity is larger than that of the amide I in the fully extended C_5 conformation. This phenomenon is contrary to the expectation that the amide I intensity is larger than that of the amide II, as often mentioned in the literature but reasonably explained in our study.

■ ASSOCIATED CONTENT

S Supporting Information. Ramachandran plots of molecular dynamics trajectories and normal-mode analysis of $\text{Ac}(\text{Deg})_n\text{-OtBu}$ ($n = 2–5$) and $\text{Ac}(\text{Gly})_5\text{-OtBu}$. This material is available free of charge via the Internet at <http://pubs.acs.org>.

■ AUTHOR INFORMATION

Corresponding Author

*E-mail: nhge@uci.edu. Phone: 949-824-1263. Fax: 949-824-8571.

■ ACKNOWLEDGMENT

We thank Yang Han for experimental assistance. This research was supported by grants from the U.S. National Science Foundation (CHE-0802913, DMS-0835863, and CHE-1013071).

■ REFERENCES

- (1) Toniolo, C.; Formaggio, F.; Kaptein, B.; Broxterman, Q. B. *Synlett* **2006**, 1295–1310.
- (2) Tanaka, M. *Chem. Pharm. Bull.* **2007**, 55, 349–358.
- (3) Kaul, R.; Balaram, P. *Bioorg. Med. Chem.* **1999**, 7, 105–117.
- (4) Toniolo, C.; Crisma, M.; Formaggio, F.; Peggion, C. *Biopolymers* **2001**, 60, 396–419.
- (5) Toniolo, C.; Benedetti, E. *Macromolecules* **1991**, 24, 4004–4009.
- (6) Paterson, Y.; Rumsey, S. M.; Benedetti, E.; Némethy, G.; Scheraga, H. A. *J. Am. Chem. Soc.* **1981**, 103, 2947–2955.
- (7) Venkataram, B. V.; Balaram, P. *Crit. Rev. Biochem. Mol. Biol.* **1984**, 16, 307–348.
- (8) Toniolo, C.; Bonora, G. M.; Barone, V.; Bavoso, A.; Benedetti, E.; Di Blasio, B.; Grimaldi, P.; Lelj, F.; Pavone, V.; Pedone, C. *Macromolecules* **1985**, 18, 895–902.
- (9) Karle, I. L.; Balaram, P. *Biochemistry* **1990**, 29, 6747–6756.
- (10) Kennedy, D. F.; Crisma, M.; Toniolo, C.; Chapman, D. *Biochemistry* **1991**, 30, 6541–6548.
- (11) Toniolo, C.; Crisma, M.; Bonora, G. M.; Benedetti, E.; Di Blasio, B.; Pavone, V.; Pedone, C.; Santini, A. *Biopolymers* **1991**, 31, 129–138.
- (12) Silva, R. A. G. D.; Yasui, S. C.; Kubelka, J.; Formaggio, F.; Crisma, M.; Toniolo, C.; Keiderling, T. A. *Biopolymers* **2002**, 65, 229–243.
- (13) Crisma, M.; Andreetto, E.; De Zotti, M.; Moretto, A.; Peggion, C.; Formaggio, F.; Toniolo, C. *J. Pept. Sci.* **2007**, 13, 190–205.
- (14) Benedetti, E.; Barone, V.; Bavoso, A.; Blasio, B. D.; Lelj, F.; Pavone, V.; Pedone, C.; Bonora, G. M.; Toniolo, C.; Leplawy, M. T.; Kaczmarek, K.; Redlinski, A. *Biopolymers* **1988**, 27, 357–371.
- (15) Toniolo, C.; Bonora, G. M.; Bavoso, A.; Benedetti, E.; Blasio, B. D.; Pavone, V.; Pedone, C.; Barone, V.; Lelj, F.; Leplawy, M. T.; Kaczmarek, K.; Redlinski, A. *Biopolymers* **1988**, 27, 373–379.
- (16) Galdecki, Z.; Luciak, B.; Kaczmarek, K.; Leplawy, M. T.; Redlinski, A. S. *Monatsh. Chem.* **1992**, 123, 993–998.
- (17) Benedetti, E.; Pedone, C.; Pavone, V.; Di Blasio, B.; Saviano, M.; Fattorusso, R.; Crisma, M.; Formaggio, F.; Bonora, G. M.; Toniolo, C.; Kaczmarek, K.; Redlinski, A. S.; Leplawy, M. T. *Biopolymers* **1994**, 34, 1409–1418.
- (18) Prasad, S.; Rao, R. B.; Bergstrand, H.; Lundquist, B.; Becker, E. L.; Balaram, P. *Int. J. Pept. Protein Res.* **1996**, 48, 312–318.
- (19) Tanaka, M.; Imawaka, N.; Kurihara, M.; Suemune, H. *Helv. Chim. Acta* **1999**, 82, 494–510.
- (20) Kaul, R.; Banumathi, S.; Velmurugan, D.; Ravikumar, K.; Rao, R. B.; Balaram, P. *J. Pept. Res.* **2000**, 55, 271–278.
- (21) Benedetti, E.; Toniolo, C.; Hardy, P.; Barone, V.; Bavoso, A.; Di Blasio, B.; Grimaldi, P.; Lelj, F.; Pavone, V.; Pedone, C.; Bonora, G. M.; Lingham, I. *J. Am. Chem. Soc.* **1984**, 106, 8146–8152.
- (22) Bonora, G. M.; Toniolo, C.; Di Blasio, B.; Pavone, V.; Pedone, C.; Benedetti, E.; Lingham, I.; Hardy, P. *J. Am. Chem. Soc.* **1984**, 106, 8152–8156.
- (23) Di Blasio, B.; Pavone, V.; Isernia, C.; Pedone, C.; Benedetti, E.; Toniolo, C.; Hardy, P. M.; Lingham, I. *N. J. Chem. Soc., Perkin Trans. 2* **1992**, 523–526.
- (24) Karle, I. L.; Kaul, R.; Rao, R. B.; Raghothama, S.; Balaram, P. *J. Am. Chem. Soc.* **1997**, 119, 12048–12054.
- (25) Barone, V.; Lelj, F.; Bavoso, A.; Di Blasio, B.; Grimaldi, P.; Pavone, V.; Pedone, C. *Biopolymers* **1985**, 24, 1759–1767.
- (26) Krimm, S.; Bandekar, J. *Adv. Protein Chem.* **1986**, 38, 181–364.
- (27) Bandekar, J. *Biochim. Biophys. Acta* **1992**, 1120, 123–143.
- (28) Barth, A.; Zscherp, C. *Q. Rev. Biophys.* **2002**, 35, 369–430.
- (29) Cho, M. *Chem. Rev.* **2008**, 108, 1331–1418.
- (30) Hamm, P.; Helbing, J.; Bredenbeck, J. *Annu. Rev. Phys. Chem.* **2008**, 59, 291–317.
- (31) Ganim, Z.; Chung, H. S.; Smith, A. W.; DeFlores, L. P.; Jones, K. C.; Tokmakoff, A. *Acc. Chem. Res.* **2008**, 41, 432–441.
- (32) Kim, Y. S.; Hochstrasser, R. M. *J. Phys. Chem. B* **2009**, 113, 8231–8251.
- (33) Zhuang, W.; Hayashi, T.; Mukamel, S. *Angew. Chem., Int. Ed.* **2009**, 48, 3750–3781.
- (34) Hunt, N. T. *Chem. Soc. Rev.* **2009**, 38, 1837–1848.
- (35) Maekawa, H.; Toniolo, C.; Moretto, A.; Broxterman, Q. B.; Ge, N.-H. *J. Phys. Chem. B* **2006**, 110, 5834–5837.
- (36) Maekawa, H.; Toniolo, C.; Broxterman, Q. B.; Ge, N.-H. *J. Phys. Chem. B* **2007**, 111, 3222–3235.
- (37) Sul, S.; Karauskaj, D.; Jiang, Y.; Ge, N.-H. *J. Phys. Chem. B* **2006**, 110, 19891–19905.
- (38) Sengupta, N.; Maekawa, H.; Zhuang, W.; Toniolo, C.; Mukamel, S.; Tobias, D. J.; Ge, N.-H. *J. Phys. Chem. B* **2009**, 113, 12037–12049.
- (39) Rubtsov, I. V.; Wang, J.; Hochstrasser, R. M. *Proc. Natl. Acad. Sci. U.S.A.* **2003**, 100, 5601–5606.
- (40) DeFlores, L. P.; Ganim, Z.; Ackley, S. F.; Chung, H. S.; Tokmakoff, A. *J. Phys. Chem. B* **2006**, 110, 18973–18980.
- (41) Bloem, R.; Dijkstra, A. G.; Jansen, T. I. C.; Knoester, J. *J. Chem. Phys.* **2008**, 129, No. 055101.
- (42) Zanni, M. T.; Gnanakaran, S.; Stenger, J.; Hochstrasser, R. M. *J. Phys. Chem. B* **2001**, 105, 6520–6535.
- (43) Rubtsov, I. V.; Hochstrasser, R. M. *J. Phys. Chem. B* **2002**, 106, 9165–9171.
- (44) Hayashi, T.; Mukamel, S. *J. Phys. Chem. B* **2007**, 111, 11032–11046.
- (45) Choi, J.-H.; Cho, M. *Chem. Phys.* **2009**, 361, 168–175.
- (46) Maekawa, H.; De Poli, M.; Toniolo, C.; Ge, N.-H. *J. Am. Chem. Soc.* **2009**, 131, 2042–2043.
- (47) Maekawa, H.; De Poli, M.; Moretto, A.; Toniolo, C.; Ge, N.-H. *J. Phys. Chem. B* **2009**, 113, 11775–11786.
- (48) Maekawa, H.; Ge, N.-H. *J. Phys. Chem. B* **2010**, 114, 1434–1446.
- (49) DeFlores, L. P.; Ganim, Z.; Nicodemus, R. A.; Tokmakoff, A. *J. Am. Chem. Soc.* **2009**, 131, 3385–3391.
- (50) Torii, H.; Tasumi, M. *J. Chem. Phys.* **1992**, 96, 3379–3387.
- (51) Hamm, P.; Lim, M.; Hochstrasser, R. M. *J. Phys. Chem. B* **1998**, 102, 6123–6138.
- (52) Torii, H.; Tasumi, M. *J. Raman Spectrosc.* **1998**, 29, 81–86.
- (53) Hamm, P.; Woutersen, S. *Bull. Chem. Soc. Jpn.* **2002**, 75, 985–988.
- (54) Ham, S.; Cho, M. *J. Chem. Phys.* **2003**, 118, 6915–6922.
- (55) Ham, S.; Kim, J.-H.; Lee, H.; Cho, M. *J. Chem. Phys.* **2003**, 118, 3491–3498.
- (56) Bouř, P.; Keiderling, T. A. *J. Chem. Phys.* **2003**, 119, 11253–11262.
- (57) Hayashi, T.; Zhuang, W.; Mukamel, S. *J. Phys. Chem. A* **2005**, 109, 9747–9759.
- (58) Gorbunov, R. D.; Kosov, D. S.; Stock, G. *J. Chem. Phys.* **2005**, 122, 224904.
- (59) Jansen, T. I. C.; Dijkstra, A. G.; Watson, T. M.; Hirst, J. D.; Knoester, J. *J. Chem. Phys.* **2006**, 125, 044312.
- (60) Lin, Y. S.; Shorb, J. M.; Mukherjee, P.; Zanni, M. T.; Skinner, J. L. *J. Phys. Chem. B* **2009**, 113, 592–602.
- (61) Hayashi, T.; Mukamel, S. *J. Mol. Liq.* **2008**, 141, 149–154.
- (62) Dapprich, S.; Komáromi, I.; Byun, K. S.; Morokuma, K.; Frisch, M. J. *J. Mol. Struct.: THEOCHEM* **1999**, 461–462, 1–21.
- (63) Cheam, T. C.; Krimm, S. *J. Mol. Struct.* **1989**, 193, 1–34.
- (64) Ishida, K. P.; Griffiths, P. R. *Appl. Spectrosc.* **1993**, 47, 584–589.
- (65) Kubelka, J.; Keiderling, T. A. *J. Phys. Chem. A* **2001**, 105, 10922–10928.
- (66) Pevsner, A.; Diem, M. *Appl. Spectrosc.* **2001**, 55, 788–793.
- (67) Birkedal, H.; Schwarzenbach, D.; Pattison, P. *Chem. Commun.* **2002**, 2812–2813.
- (68) Åberg, A.; Yaremchuk, A.; Tukalo, M.; Rasmussen, B.; Cusack, S. *Biochemistry* **1997**, 36, 3084–3094.
- (69) Kaminski, Z.; Leplawy, M. T.; Olma, A.; Redlinski, A. In *Peptides 1980*, Proceedings of the 16th European Peptide Symposium, Helsingør, Denmark; Brunfeldt, K., Ed.; Scriptor: Copenhagen, 1981; pp 201–206.
- (70) Leplawy, M. T.; Kaczmarek, K.; Redlinski, A. In *Peptides: Chemistry and Biology*, Proceedings of the 10th American Peptide

Symposium, St. Louis, MO; Marcshall, G. R., Ed.; ESCOM: Leiden, 1988; pp 239–241.

(71) Maekawa, H.; Formaggio, F.; Toniolo, C.; Ge, N.-H. *J. Am. Chem. Soc.* **2008**, *130*, 6556–6566.

(72) Zanni, M. T.; Ge, N.-H.; Kim, Y. S.; Hochstrasser, R. M. *Proc. Natl. Acad. Sci. U.S.A.* **2001**, *98*, 11265–11270.

(73) Phillips, J. C.; Braun, R.; Wang, W.; Gumbart, J.; Tajkhorshid, E.; Villa, E.; Chipot, C.; Skeel, R. D.; Kalé, L.; Schulten, K. *J. Comput. Chem.* **2005**, *26*, 1781–1802.

(74) Cornell, W. D.; Cieplak, P.; Bayly, C. I.; Gould, I. R.; Merz, K. M.; Ferguson, D. M.; Spellmeyer, D. C.; Fox, T.; Caldwell, J. W.; Kollman, P. A. *J. Am. Chem. Soc.* **1995**, *117*, 5179–5197.

(75) Hornak, V.; Abel, R.; Okur, A.; Strockbine, B.; Roitberg, A.; Simmerling, C. *Proteins: Struct., Funct., Bioinf.* **2006**, *65*, 712–725.

(76) Torras, J.; Zanuy, D.; Crisma, M.; Toniolo, C.; Betran, O.; Alemán, C. *Biopolymers* **2008**, *90*, 695–706.

(77) Martyna, G. J.; Tobias, D. J.; Klein, M. L. *J. Chem. Phys.* **1994**, *101*, 4177–4189.

(78) Feller, S. E.; Zhang, Y.; Pastor, R. W.; Brooks, B. R. *J. Chem. Phys.* **1995**, *103*, 4613–4621.

(79) Darden, T.; York, D.; Pedersen, L. *J. Chem. Phys.* **1993**, *98*, 10089–10092.

(80) Ryckaert, J.-P.; Ciccotti, G.; Berendsen, H. J. C. *J. Comput. Phys.* **1977**, *23*, 327–341.

(81) Kim, J.-H.; Cho, M. *Bull. Korean Chem. Soc.* **2003**, *24*, 1061–1068.

(82) Frisch, M. J.; Trucks, G. W.; Schlegel, H. B.; Scuseria, G. E.; Robb, M. A.; Cheeseman, J. R.; Montgomery, J. A., Jr.; Vreven, T.; Kudin, K. N.; Burant, J. C.; Millam, J. M.; Iyengar, S. S.; Tomasi, J.; Barone, V.; Mennucci, B.; Cossi, M.; Scalmani, G.; Rega, N.; Petersson, G. A.; Nakatsuji, H.; Hada, M.; Ehara, M.; Toyota, K.; Fukuda, R.; Hasegawa, J.; Ishida, M.; Nakajima, T.; Honda, Y.; Kitao, O.; Nakai, H.; Klene, M.; Li, X.; Knox, J. E.; Hratchian, H. P.; Cross, J. B.; Bakken, V.; Adamo, C.; Jaramillo, J.; Gomperts, R.; Stratmann, R. E.; Yazyev, O.; Austin, A. J.; Cammi, R.; Pomelli, C.; Ochterski, J. W.; Ayala, P. Y.; Morokuma, K.; Voth, G. A.; Salvador, P.; Dannenberg, J. J.; Zakrzewski, V. G.; Dapprich, S.; Daniels, A. D.; Strain, M. C.; Farkas, O.; Malick, D. K.; Rabuck, A. D.; Raghavachari, K.; Foresman, J. B.; Ortiz, J. V.; Cui, Q.; Baboul, A. G.; Clifford, S.; Ciosowski, J.; Stefanov, B. B.; Liu, G.; Liashenko, A.; Piskorz, P.; Komaromi, I.; Martin, R. L.; Fox, D. J.; Keith, T.; Al-Laham, M. A.; Peng, C. Y.; Nanayakkara, A.; Challacombe, M.; Gill, P. M. W.; Johnson, B.; Chen, W.; Wong, M. W.; Gonzalez, C.; Pople, J. A. *Gaussian 03*; Gaussian, Inc.: Wallingford, CT, 2004.

(83) Bouteiller, Y.; Gillet, J.-C.; Grégoire, G.; Schermann, J. P. *J. Phys. Chem. A* **2008**, *112*, 11656–11660.

(84) Ganim, Z.; Tokmakoff, A. *Biophys. J.* **2006**, *91*, 2636–2646.

(85) Dijkstra, A. G.; Knoester, J. *J. Phys. Chem. B* **2005**, *109*, 9787–9798.

(86) Hochstrasser, R. M.; Whiteman, J. D. *J. Chem. Phys.* **1972**, *56*, 5945–5958.

(87) Fidder, H.; Knoester, J.; Wiersma, D. A. *J. Chem. Phys.* **1991**, *95*, 7880–7890.

(88) Bouř, P.; Michalík, D.; Kapitan, J. *J. Chem. Phys.* **2005**, *122*, 144501.

(89) Zhuang, W.; Abramavicius, D.; Hayashi, T.; Mukamel, S. *J. Phys. Chem. B* **2006**, *110*, 3362–3374.

(90) Kobko, N.; Dannenberg, J. J. *J. Phys. Chem. A* **2003**, *107*, 6688–6697.